A Discrete and Hybrid Approach to Predicting Diametrical Errors in Slender Shaft Turning

Xiaoyi Fang

A Thesis

in

The Department

of

Mechanical, Industrial, and Aerospace Engineering

Presented in Partial Fulfillment of the Requirements

for the Degree of

Master of Applied Science (Mechanical Engineering) at

Concordia University

Montreal, Quebec, Canada

October 2020

CONCORDIA UNIVERSITY

School of Graduate Studies

This is to certify that the thesis prepared

By: **Xiaoyi Fang**

Entitled: **A Discrete and Hybrid Approach to Predicting Diametrical Errors in Slender Shaft Turning**

and submitted in partial fulfillment of the requirements for the degree of

Master of Applied Science (Mechanical Engineering)

complies with the regulations of the University and meets the accepted standards with respect to originality and quality.

Signed by the final examining committee:

_____ Chair
Dr. Y. Zhang

_____ Examiner
Dr. L. Wang

_____ Examiner
Dr. Y. Zhang

_____ Supervisor
Dr. Z. C. Chen

Approved by _____ Chair of Department or Graduate Program Director
Dr. Mamoun Medraj

_____Dean of Faculty
Dr. Mourad Debbabi

Date _____
November 24, 2020

ABSTRACT

A Discrete and Hybrid Approach to Predicting Diametrical Errors in Slender Shaft Turning

Xiaoyi Fang

Slender shafts have a high length-to-radius ratio, low rigidity, and are often machined on a lathe to comply with the tight tolerance requirement. The machined accuracy for slender shafts, which is reflected in its diametrical deviations, is very sensitive to forces exerted by the cutting tool. To compensate for such errors effectively, this research aims to predict the diametrical deviations in slender shafts turning process efficiently and accurately. First, based on the geometric principles in turning processes, a mathematical model is built, in order to relate the given depth of cut and the shaft deflection due to the force of the cutting tool to the diametrical deviations. Then a novel finite element model considering the practical machining situation is developed to solve the aforementioned mathematical model. Compared with traditional finite element methods, the novel method addresses the interaction between the depth of cut and the cutting force throughout the machining process. A discretization method is employed to handle this coupled interaction. The approach to diametrical deviations prediction is verified with the experimental data and situations for various machining parameters and stock materials are discussed. The approach is also extended to the generic case involving workpieces with different diameters features along the shaft.

Acknowledgments

I hereby wish to express my sincerest gratitude and appreciation to my supervisor, Dr. Chevy Chen, for his priceless guidance and insights that lead me through this research.

I would also like to thank my fellows in our lab for their accompaniment and generous support and ideas when I encountered problems in the past two years. My special thanks go to Stephen Fang, who is the senior researcher in our team, for his daily advice on this work.

Finally, I want to show my deepest gratitude to my parents, who support and guide me wherever I am, whatever I do, and whenever I need them.

Table of Contents

List of Figures

List of Tables

Chapter 1 Introduction

1.1 Background

Slender shafts play a critical role in the manufacturing industry. Their wide application includes aero-engines, automobile transmission system, photoelectric masts in submarines, extensible support structures of satellites, and so on. In the manufacturing industry, a shaft is a rotating machine element with circular in cross-sections and a slender shaft has a length-to-diameter ratio larger than 10 [1]. Due to these characteristics, slender shafts have relatively low rigidity and is prone to deform during manufacturing. For slender shafts with tight tolerance requirements, a lathe is utilized to turn their external or internal diameters. In the turning process, the shaft is first clamped at one end with the chuck or collet, the other end fixed with a center, and then the cutting tool is fed along the shaft to remove the unwanted material. Since slender shafts are relatively flexible, the cutting tool can deform the shaft from its nominal dimension. Such deformation, also known as diametrical machining deviation, can reach up to 0.1mm. Unfortunately, in today's manufacturing industry, a shaft with this deviation is disqualified. Therefore, methods are needed to eliminate or levitate such deviations.

Practically, the deflection of the shaft is inherent and cannot completely be eliminated even with nowadays advanced clamping methods. Thus, engineers usually take another route to achieve parts that comply with the tight tolerance requirement. By using modern computer-aided manufacturing (CAM) system and computer-numerical controlled (CNC) machines, the following procedures are not uncommon to compensate for the deviation of the machined part: 1) measure the part, 2) decide the number of deviations to be compensated, 3) reprogram the cutter paths in CAM system and 4) rework the part on a CNC machine. In practice, the part deviates from its nominal dimension due to the combined effects of a part material, machining condition, cutting tool, and machining parameters. The lack of knowledge on the quantified deviation during the machining process leads to a conservative selection of compensation values when the second steps of the above procedures are performed. As a result, this whole process

will need to iterate multiple times until the desired part dimension is reached. Frequently, a set of compensation values can be wrongly selected since the machining conditions will change during machining. This will render the part useless, which happens especially frequently in the process of slender shafts turning.

To solve this problem, the dimensional deviation (usually diametrical deviation) of the slender shaft during the turning process should be predicted accurately. The predicted values can be used as guidance for re-computing the cutter paths. In order to understand the current techniques to predict the diametrical deviation, a literature review is conducted.

1.2 Literature review

Researches of slender shaft turning have been conducted since many years ago. A.-V. PHAN et al [1] developed a model of computing part deflections considered all three cutting force components and three usual methods of mounting workpieces in a turning process. Rene Mayer and Anh-Vu Phan [2] presented a computationally effective model of predicting diameter errors in bar turning considering the deflection of the whole machine-workpiece-tool system. An approach shown to obtaining the accurate force in bar turning has been proposed by D.A. Stephenson and P.Bandyopadhyay [7]. Bodi Cui and Rongdi Han [8] built an artificial neural network model to describe the relationship between cutting parameters and dimensional errors in the slender bar turning process. L. Kops [9] provided a non-dimensional procedure generalizing the results for practical applications. A real-time error compensation system has been developed to reduce the cutting force induced planar error of a two-axis turning center by Yang, S. Yuan, J. and Ni, J [10]. A united model consists of three components: geometric analysis of diametrical error, finite element model of workpiece deflection, and statistical model of cutting forces for predicting diametrical error of slender bar has been proposed by Jianliang, G. and Rongdi, H [11]. Carrino, L., Giorleo, G., Polini, W. and Prisco, U. proposed a model that can estimate the real depth of cut along the workpiece axis, the components of the cutting force, the spatial

orientation of the cutting force, and the workpiece axis displacement [12]. Wilhelm, R.G. used a controlled series of experiments to test the efficacy of these performance tests in the prediction of part form errors [13]. Polini, W. and Prisco, U. defined a new model to estimate a bar diameter error due to the deflection of the tool, of the workpiece-holder, and the workpiece [14]. An on-line ultrasonic measurement system that operates in the presence of cutting fluid is employed for workpiece diameter measurement in the research of Shawky, A.M., and Elbestawi, M.A. [15]. Fan, C., Collins Jr, E.G., Liu, C. and Wang, B. [16] studied an in-process measurement and control system called radial error feedback control (REFC) for bar turning in CNC turning centers. Cui, B.D. and Guo, J.L. [17] used a radial basis function neural network to investigate dimensional errors in slender bar turning. Phan, A.V., Baron, L., Mayer, J.R.R. and Cloutier, G. made a great improvement compared to their previous work. They determined the workpiece deflections in which the part holder stiffness is directly included and shear deformation effect is taken into account [18]. In 1994, Kops, L., Gould, M. and Mizrach, M. found the key to predict diameter error in tuning is to consider the equilibrium between the workpiece deflection and the cutting depth [19]. Most of the above methods applied finite element methods to facilitate the prediction of workpiece deflection in turning. Thus, the general idea of the finite element method is reviewed.

1.3 Finite element method (FEM)

In a sense, engineering problems are mathematic models with physics constraints. Equations can be derived from the fundamental geometry and physics principles to describe the problem. The finite element method is a numerical procedure that can be used to obtain solutions to a large class of engineering problems. Finite element methods include the following kernel steps [3].

1) Discretization of the large solution domain in smaller domains. Specifically, these smaller domains are nodes and elements.
2) Use a continuous function to represent the physical behavior of an element, e.g., use Hooke's law to represent the change of length of the element.
3) Establish equations for an element.

4) Assemble the elements in order to represent the whole problem. The assembled matrix known as the global stiffness matrix is constructed in this step.
5) Apply boundary conditions (e.g. constraints), initial conditions, and loading to the problem
6) Solve a set algebraic equation simultaneously for the results of each node (e.g. the displacement in each node).
7) Obtain further information.

Step 1 to 5 is known as the preprocessing phase. Step 6 is the solution phase and Step 7 is the postprocessing phase. Since this work focuses on obtaining the deflection of the slender shaft, Step 1 to 6 are needed.

1.4 Slender shaft manufacturing

A shaft can be made with different methods. For mass production of shafts with very low diametrical tolerance, rolling and casting can be used. In the case of shafts with tight tolerance, turning is more favorable. Turning is a process of machining an external cylindrical and conical surface. Although multi-purpose CNC machines such as mill-turn machines can be used for the turning process, this process is usually performed on a machine tool called a lathe, with a cutting tool [5]. In the turning process, the workpiece is rotated and a single-point cutting tool is fed longitudinally into the workpiece [16].

The slender shaft is defined as the shaft with a ratio of length and diameter of its cross-section that is more than 10. Due to these characteristics, although the material of the slender shafts can be hard, a salient feature of slender shafts is their relatively low rigidity. So they are easy to deform during manufacturing. Therefore, extra care must be applied when machining such shafts. To increase the rigidity of the part, a hydraulic tailstock and a hydraulic steady rest are used together to provide extra support (see Fig 1.1). The shaft is clamped with the chuck at one end and is held in place by the tailstock at the other end. For most of the modern CNC machines, the

center of the chuck and the tailstock can be manually aligned with high accuracy before machining (the requirement for concentricity is usually no more than 0.002mm for extremely tight tolerance parts) [4]. The position of the steady rest is defined by the engineer based on prior experience.

The slender shaft will still undergo deflection even with this current setup. This leads to the deviation of diameters between the machined part and the design part. A common practice is to measure the diameter of the shaft once it is machined. The deviation between the actual diameter and the required diameter is found and the tool path will be adjusted according to that deviation and the past experience. This practice will be repeated many times until the part has complied with the specified tolerance. This research aims to provide a scientific way to predict such deflection before machining. That way, the traditional blind-folded trial and error approach can be avoided.

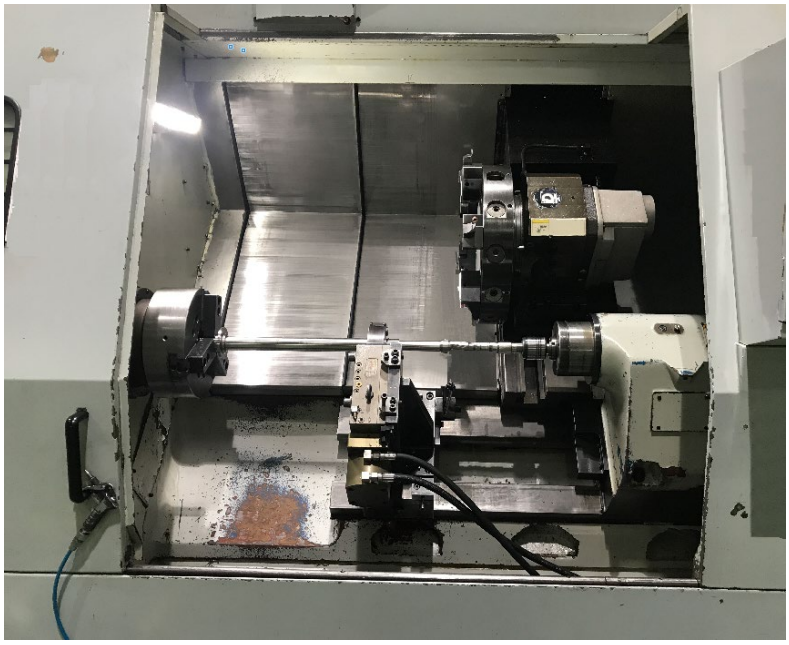

Fig 1.1 Slender shaft turning

1.5 Research objectives

The objectives of this thesis focus on precisely and efficiently predicting diametrical errors in slender shaft turning, and the work can be concluded in following aspects:

- A comprehensive computational model considered the change of the depth of cut and the cutting force during the machining process is developed for predicting diametrical errors in slender shaft turning.
- A computational model for predicting diameter error adapted for slender shafts with different features and the positions of the steady rest is built.

The rest of the thesis is organized as the followings. In Chapter 2, the geometric principle of the slender shafts turning process is considered and the diametrical deviation of the machined part is expressed in terms of the depth of cut and the deflection of the shaft. In Chapter 3, a new FEM model is developed as to solve for the deflection of the shaft described in Chapter 2. Verification and discussion of such a FEM model are also presented. 0 describes a generic diametrical error prediction model for the featured slender shaft and its application. Chapter 6 gives the conclusions and the recommendation of future work based on the current research.

Chapter 2 Geometry Model of Slender Shafts Turning Processes

2.1 Exhibition of diametrical deviation in slender shafts turning processes

In slender shaft turning, the workpiece tends to drift away from the tool under cutting forces because of its high length-diameter ratio. The deflection caused by the cutting forces will induce differences between nominal cutting depth and actual cutting depth. This difference, in turn, causes the diametrical deviation in slender shaft turning [7].

As illustrated in Fig 2.1, a slender shaft is clamped by the chuck-center method. As the workpiece rotates and the single-point cutting tool feeds longitudinally along the workpiece, the workpiece is machined. During machining, the shaft undergoes deflection. In Fig 2.1, the translucent and straight shaft is the nominal slender shaft. This is how this slender shaft is supposed to be. In practice, the shaft is bent and is illustrated as the solid shaft In Fig 2.1. The bending deformation occurs under the influence of the cutting forces F_t and F_r in actual machining.

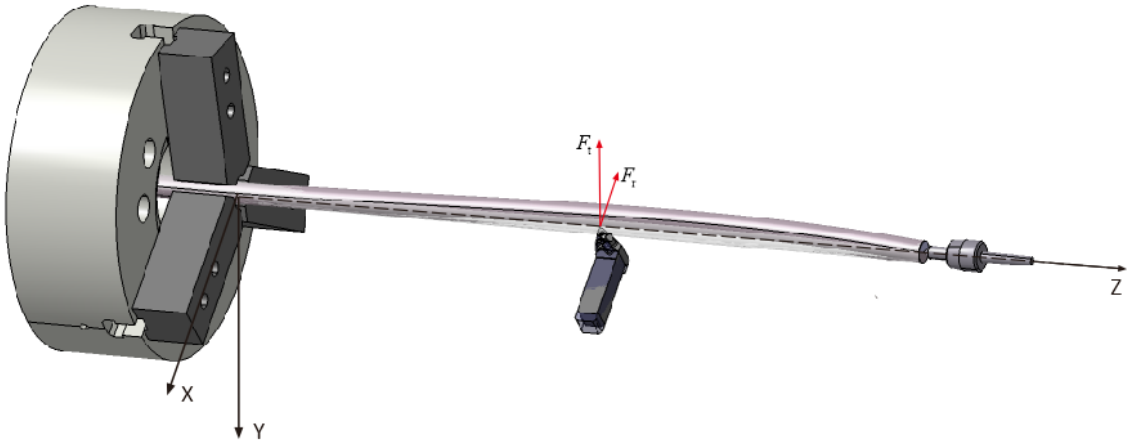

Fig 2.1 Deflection caused by cutting forces in slender shafts turning processes

A follow rest and more often a steady rest is used to counter the slender shaft from the deflection caused by the cutting tool. Unfortunately, according to Guo Jiangliang et al's [7] research, the

diametrical error still exists and cannot be ignored in the machining even with the addition of a steady rest.

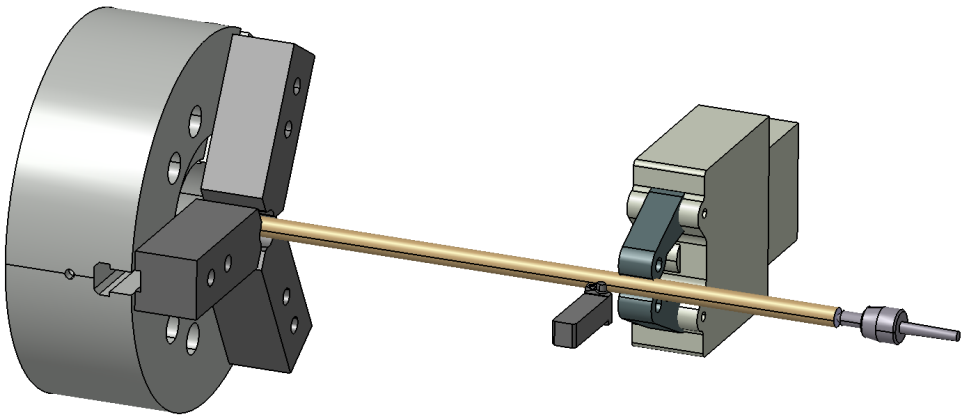

Fig 2.2 Slender shaft turning processes with a steady rest

In summary, the diametrical deviation of the slender shaft is due to the effect of the cutting force and such deviations cannot be neglected.

2.2 Geometry principles and the representation of the diametrical deviation

In order to model the diametrical deviation, the geometric principle of the slender shaft turning process is considered. The diametrical deviation can be considered to be caused by the deflections of the machine-workpiece-tool system. This deviation can be expressed in the part cross-section contains the cutting point. Compared to the workpiece and the tool, the machine can be considered to be rigid enough and it does not contribute to the overall shaft deflection [14]. Hence, in this work, only the deflections of the workpiece and the tool due to the cutting forces are analyzed.

To express the relevant terms, a coordinate system is defined in Fig 2.3. The origin of the coordinate system is defined at the center of the chuck end face. The Z-axis is along the chuck

axis and the positive Z-direction is from chuck to center. The X-axis is perpendicular to the Z-axis, and the positive X-direction is the direction where the tool moves away from the workpiece in the radial direction. The Y-axis is defined according to the right-hand rule.

In oblique turning, the cutting force can be broken down into three component forces along the three coordinate axes. They are the radial force F_r along the X-axis, the tangential force F_t along the Y-axis, the axial force F_a along Z-axis. In the study of how the deflection occurred in slender shaft turning, the radial force F_r and the tangential force F_t both contribute to the bending deflection in slender shaft turning. These two forces largely contribute to the diametrical deviation. Meanwhile, the axial force F_a causes the compression deformation. According to the theory of material mechanics [25], the compression deformation is about 1/1000 of the bending deformation. Therefore, in this research, the axial force F_a and the compression deformation caused by the axial force F_a are not considered.

As shown in Fig 2.3, u_x is the deflection in the X-direction under the influence of the radial force F_r . u_y is the deflection in the X-direction under the influence of the tangential force F_t .

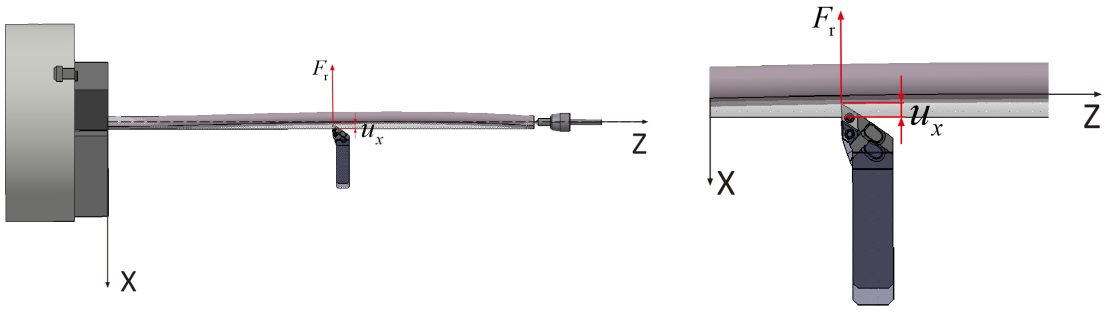

(a)

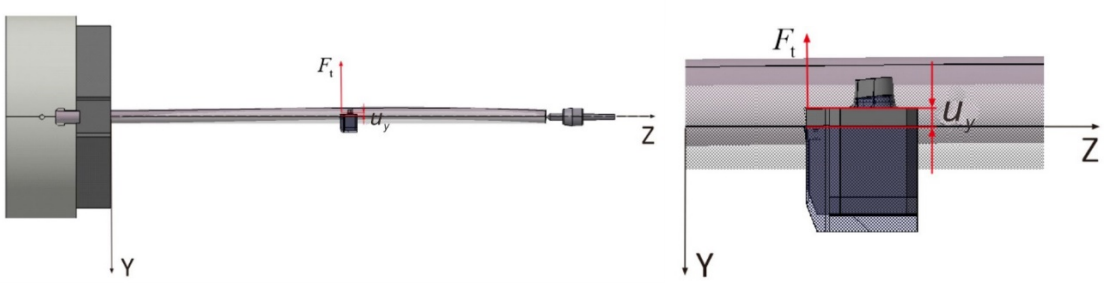

(b)

Fig 2.3 Deflection causes by cutting forces in (a) the radial direction and (b) the tangential direction

The geometry principle of the slender shafts in the turning process is illustrated in the cross-section view. As shown in Fig 2.4, in the ideal situation, the bigger circle in light grey is the original cross-section which has not been cut and R is its radius. The smaller circle in dark grey is the nominal cross-section. This is the ideal cross-section after turning and its diameter is D_n. d_n is the depth of cut. Meanwhile, since these two circles are concentric in the ideal situation, the point O is the center of both the original cross-section and the nominal cross-section in Fig 2.4.

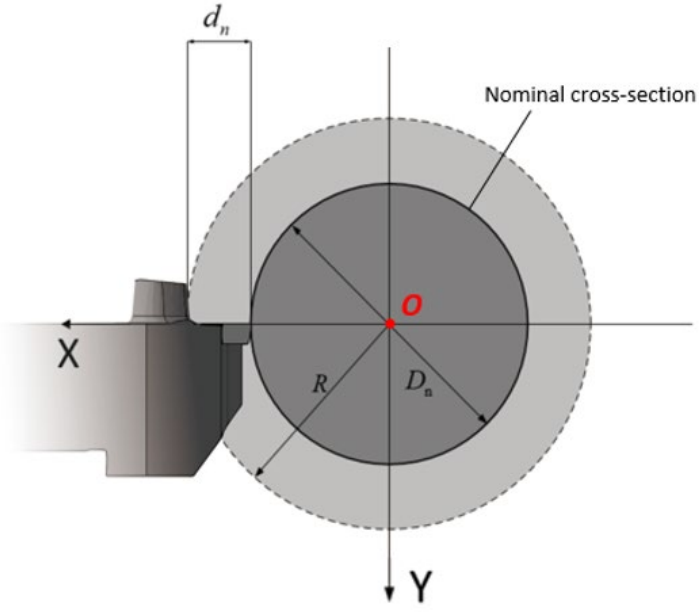

Fig 2.4 Nominal cross-section in slender shaft turning

However, in actual manufacturing, the deflection caused by the interaction between the workpiece and the cutter cannot be ignored. The actual slender shaft cross-section when being machined is shown in Fig 2.5. The bigger solid circle is the original cross-section which has not been cut. The smaller circle with a hatch fill is the actual cross-section in slender shaft turning and D_p is the predicted diameter of the actual cross-section. As displacement occurred on the workpiece, three main changes can be observed: 1) the nominal depth of cut changes from d_n to d_p; 2) the center of the cross-section moves from point O to O'; and 3) the machined cross-section diameter changes from D_n to D_p. The difference between D_n and D_p is defined as the diametrical deviation in this work.

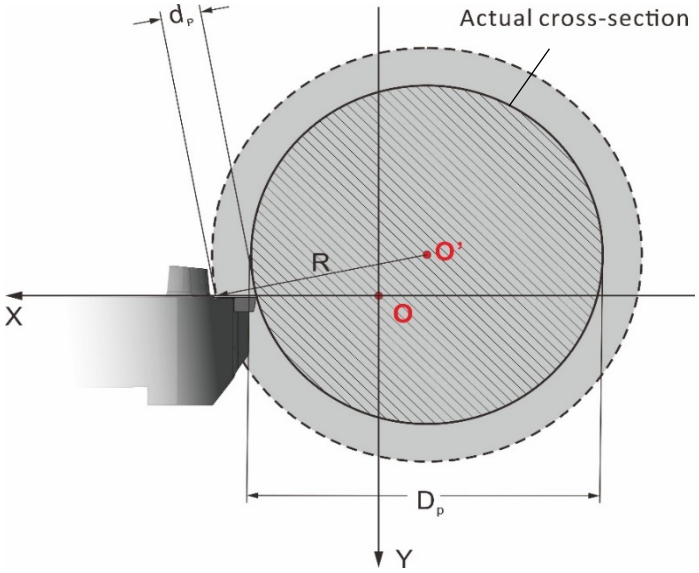

Fig 2.5 Actual cross-section in the slender shafts turning process

Since D_n is the nominal slender shaft diameter, it is specified. To obtain the diametrical deviation, D_p should be found.

As shown in Fig 2.6, the radial cutting force F_r along the X-axis causes the radial deflection u_x and the tangential cutting force F_t causes the tangential deflection u_y.

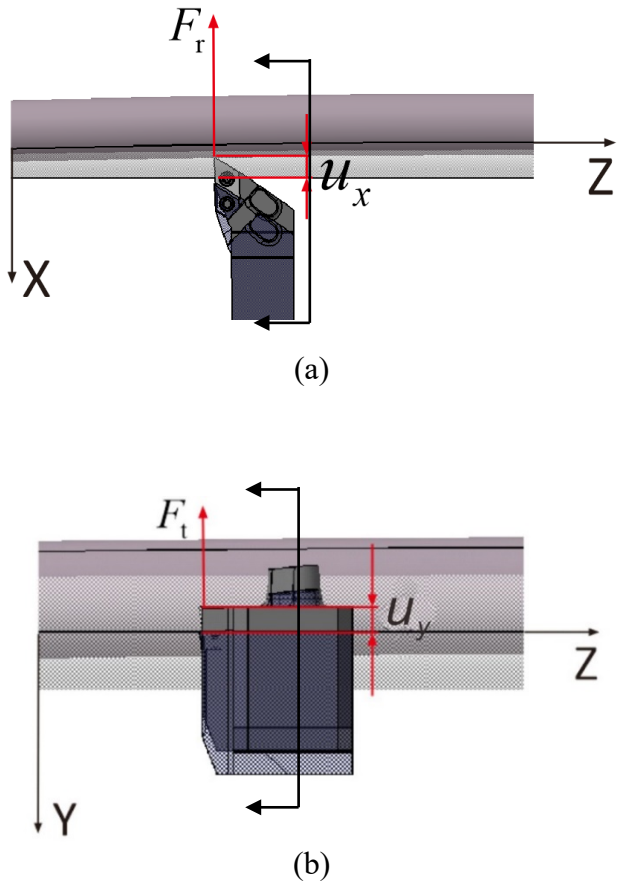

Fig 2.6 Force-deformation relationship in slender shaft turning in (a) the X-Z plane and (b) the Y-Z plane

Combining the view in Fig 2.6 and Fig 2.5, Fig 2.7 can be obtained. Fig 2.7 is also the combination of Fig 2.4 and Fig 2.5, including the original slender shaft cross-section in solid light grey, the nominal machined slender shaft cross-section in solid dark grey, and the predicted actual machined slender shaft cross-section with hatch fill. u_{wx} and u_{wy} are the workpiece deflection under the influence of the cutter in the X and Y directions separately. u_{tx} and u_{ty} are the cutter deflection under the influence of the workpiece in the X and Y directions separately. The following geometric relationships exist:

$$u_x = |u_{wx}| - |u_{tx}|$$

$$u_y = |u_{wy}| - |u_{ty}|$$

Eq. 2.1

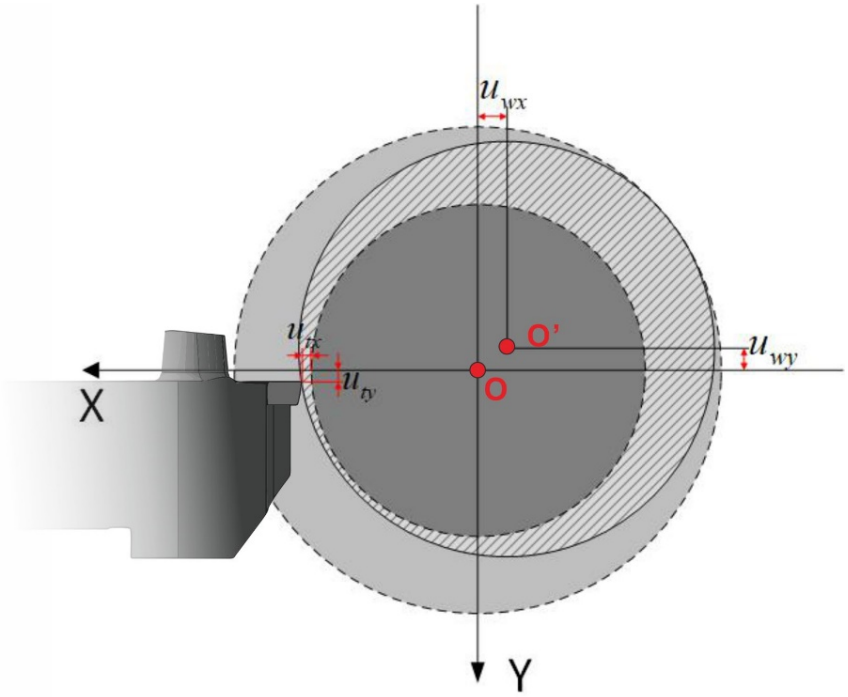

Fig 2.7 Geometrical Analysis of Diametrical error in the cross-section

Since the cutting tool is often short and rigidly mounted on the turret of the lathe, compared to the slender shaft, the cutting tool's deflection can also be ignored [6][11]. Thus, u_{tx} and u_{ty} can be ignored in this research and Eq. 2.1 can be simplified to:

$$u_x = |u_{wx}|$$

$$u_y = |u_{wy}|$$

Eq. 2.2

In Fig 2.8, u_{tx} and u_{ty} has already been ignored. $O'P$ connects the deflected slender shaft cross-section center O' and the contact point of the cutting tool and the workpiece. It is the radius of the slender shaft in the actual turning process. The length of $O'P$ can be obtained according to the Pythagorean theory if u_{wx} and u_{wy} are known.

$$2 \cdot \overline{O'P} = D_P = 2\sqrt{\left(R - d_n + |u_{wx}|\right)^2 + |u_{wy}|^2}$$

Eq. 2.3

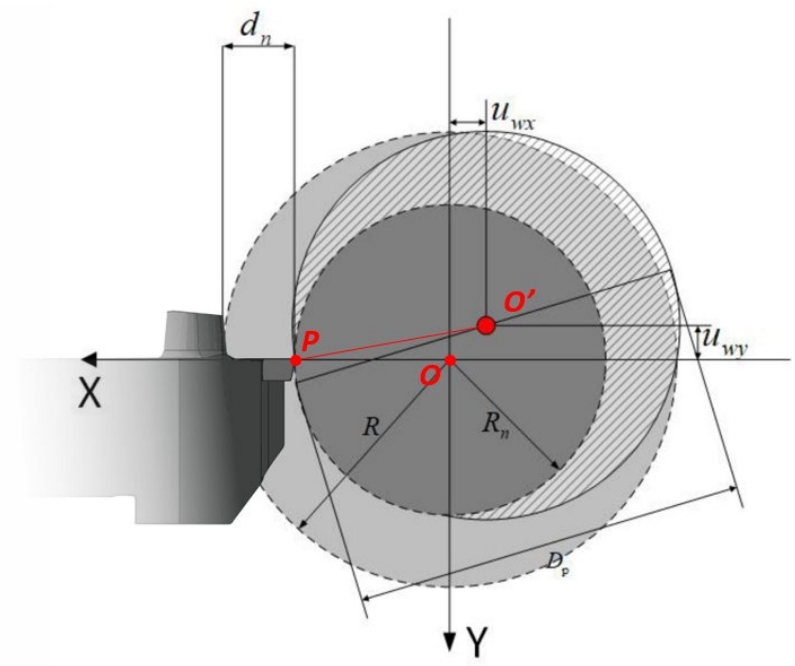

Fig 2.8 Geometrical analysis of diametrical error in the cross-section ignored the cutter deflection

u_{wx} and u_{wy} are the workpiece deflection under the influence of cutter in the X and Y directions. Therefore, u_{wx} and u_{wy} are functions of the cutting force F_r and F_t. Then Eq. 2.3 can be written as:

$$D_P = 2\sqrt{\left(R - d_n + \left|u_{wx}\left(F_r\right)\right|\right)^2 + \left|u_{wy}\left(F_t\right)\right|^2}$$

Eq. 2.4

The diametrical deviation ΔD can be obtained as：

$$\Delta D = D_p - D_n$$

Eq. 2.5

Chapter 3 Development of the Discrete and Hybrid Approach of Diametrical Deviation Prediction for Slender Shafts Turning

3.1 Introduction to traditional methods of diametrical deviation for slender shafts turning processes

Most of the previous research uses the finite element method to predict the deflection of the shaft during machining. Typically, J.R Rene Mayer [2] proposed a computationally effective model for predicting diameter errors in bar turning, considered the influence of different part holders and mounting ways. Jianliang.G and Rongdi.H [11] also developed a united model of diametrical error in slender bar turning. Firstly, they did the geometric analysis of diameter error in turning slender shaft based on the figure below:

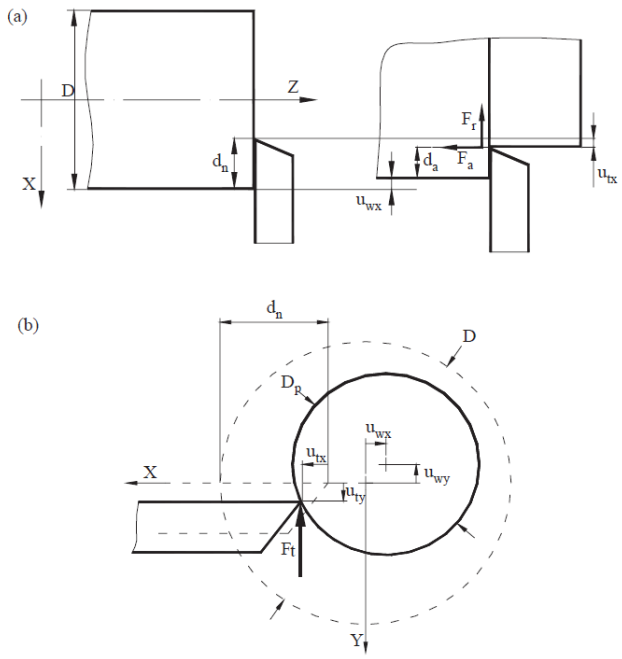

Fig 3.1 Geometric analysis in existing research [11]. (a) In the XZ plane; (b) in the XY plane

Secondly, they proposed a finite element model of workpiece deflection. Specifically, they need to discretize the bar, analyze each bar element, and then assemble the elements together, as shown in Fig 3.2, the bar was discretized in three elements in their finite element model.

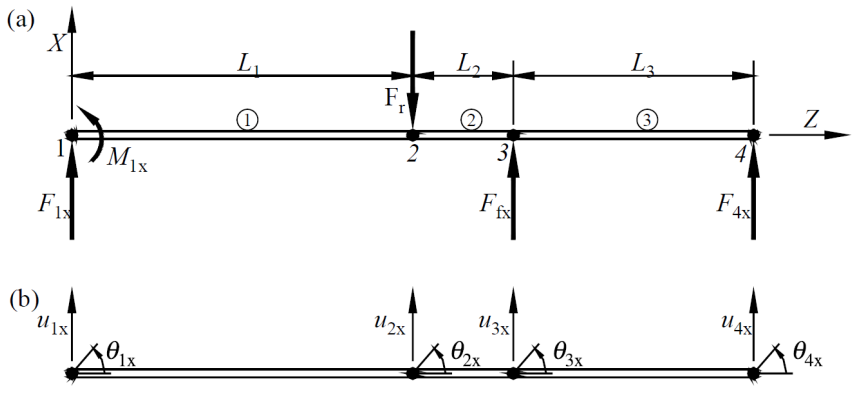

Fig 3.2 Finite element model in XZ plane [11]. (a)Boundary conditions and external forces; (b) degrees of freedom

The diametrical deviation is predicted with the numerical model based on the finite element model above, which includes: the stiffness matrix who presents the property of the slender bar, in their cases, a solid 1045 steel bar with uniform cross-sections is used; the loading vector, who reflects the loading condition of the bar, in their loading vector, constant cutting force components are used; and the displacement vector, who means the deflection of the slender shaft, contains the boundary conditions and the deformation of the bar under the influence of the cutting force.

Finally, they did an experience as shown in Fig 3.3 and proved the above method can predict the diametrical deviation without an obvious difference with the experimental results.

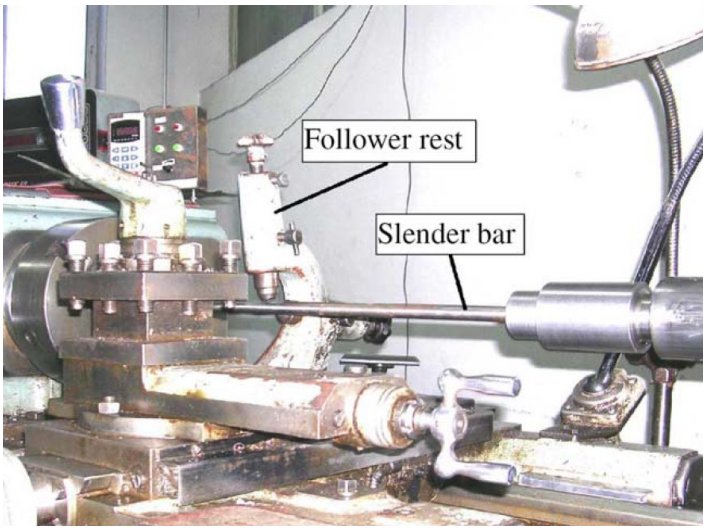

Fig 3.3 Experimental set-up [11]

3.2 Motivation to the establishment of the discrete and hybrid model

3.2.1 Analysis of the real situation

The process of slender shaft turning starts with clamping the slender shaft at the chuck in one end, and at the tailstock in the other end. At the beginning of the turning process, the slender shaft rotates at a spindle speed. Then, the cutting tool feeds towards the part until the machining is completed. In every instance, the tool is cut inside the workpiece, and therefore, the cutting force exists. At the same time, such cutting forces will deflect the workpiece. Once the workpiece is deflected, with the cutting tool at the same position radially, the depth of cut decreases. According to [26], the cutting force is proportional to the depth of cut. This means that as the depth of cut decreases, the cutting force decreases accordingly. The decreased cutting force deflects the shaft less, which in turn increases the depth of cut. As a result, the cutting force will increase again and the shaft will deflect more. This depth-of-cut/cutting force coupling effect always exists and keeps changing in the whole turning process, it will not disappear over time. And it cannot be ignored.

3.2.2 The insufficient of existing methods

Existing methods assumed the slender shaft is analyzed in a stable circumstance. At the very beginning, coupled cutting forces and depth of cut are obtained based on an optimization iterative calculation and are used directly in the turning process from the very first moment until the very last moment. Then constant cutting force and depth of cut are assumed to remain unchanged in the whole turning process. Unfortunately, this is not the case in real situations.

Additionally, in the optimization iterative calculation above, the position of the cutting tool remains the same, meaning that the distance between the chuck and the cutting tool is not changing. However, in order to cut the workpiece, the tool must be fed along the Z-axis with a feed rate. The distance between the chuck and the cutting tool keeps changing. Therefore, the stiffness used to calculate the diameter error should be updated.

In conclusion, according to the real situation, a new model for predicting the diameter error in slender shaft turning considering the changing of the cutting force and the depth of cut in different moments needs to be developed.

3.3 The basic principle for the discrete and hybrid approach

The diametrical deviation is caused by the cutting force. When the cutting tool pushes the slender shaft with the cutting force, the depth of cut decreases. According to [26], cutting force components are functions of the depth of cut. Therefore, the depth of cut and the cutting force are the functions of each other, there exists coupling between the depth of cut and the cutting force. These coupling effects and the changes of cutting forces and cutting depths in different instances during machining are the foundation of the novel model.

As shown in Fig 3.4, a slender shaft is being machined and the feed per revolution is f .

Fig 3.4 Turning of a slender shaft

The view Π is the cross-section of the slender shaft. In an ideal situation, it is illustrated in Fig 3.5.

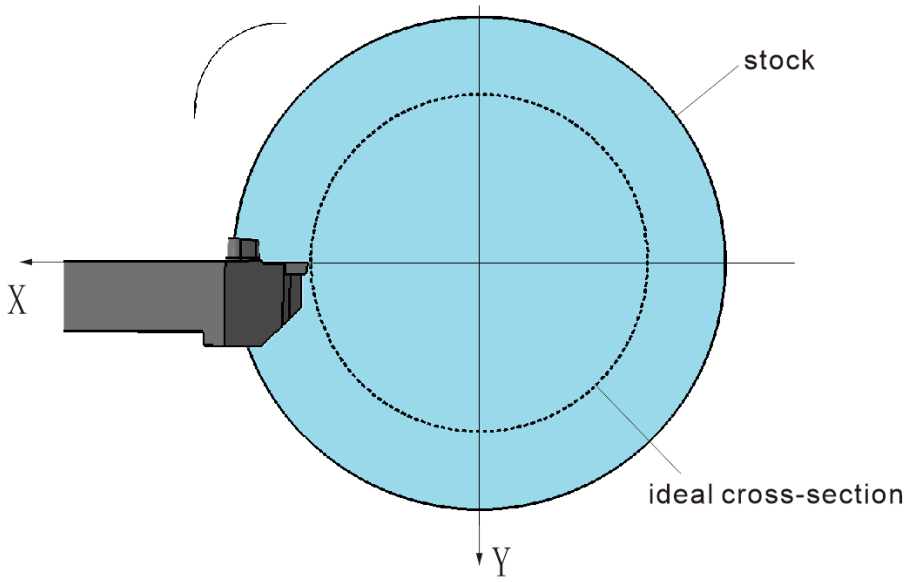

Fig 3.5 The cross-section view in the ideal situation

When the diametrical deviation is predicted with traditional methods, the cross-section is illustrated in Fig 3.6. This figure governs the whole turning process. And the actual depth of cut and cutting forces are obtained with an iterative calculation before the turning process begins.

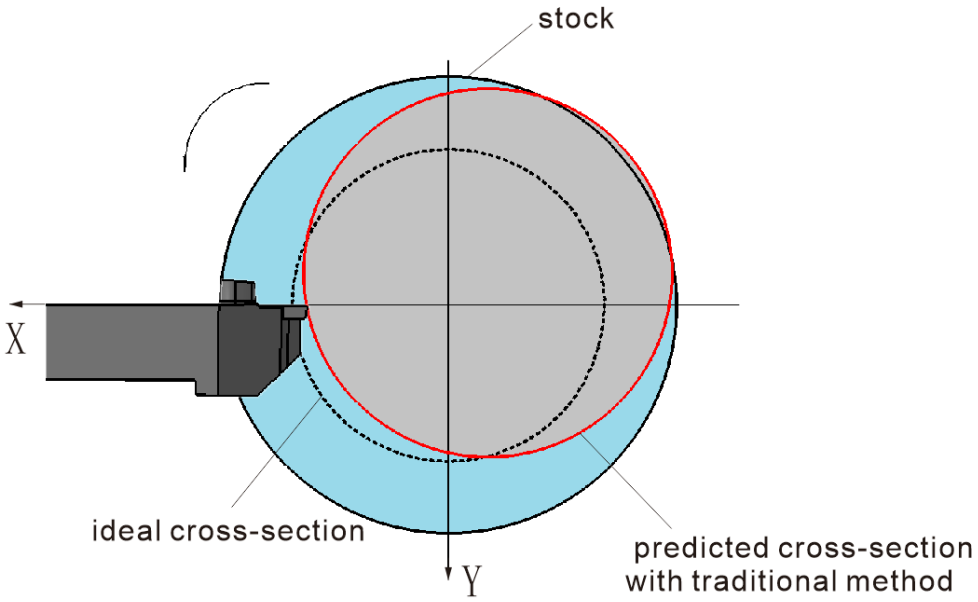

Fig 3.6 The cross-section predicted with traditional methods

In this work, the changes of cutting forces and the depth of cut at different instances are considered. Starting from the first feed per revolution, in practical situation, the depth of cut changes smoothly due to part deflections created by the push of the tool. However, within a small angle α that the part turns, the depth of cut does not change significantly. Therefore, within this small angle, we can consider the cutting force remains constant. The process for the part that turns by the small angle α is defined as one stage here. The contact point of part and tool at the very beginning is marked for the convenience of observation (see Fig 3.7).

In the first stage, the part turns a degree α (see Fig 3.7). Under the influence of the depth of cut and cutting forces in this stage, the predicted cross-section is the red circle as shown. When the tool finished turning the part in the first stage, the part turns α deg and the pink locus is formed.

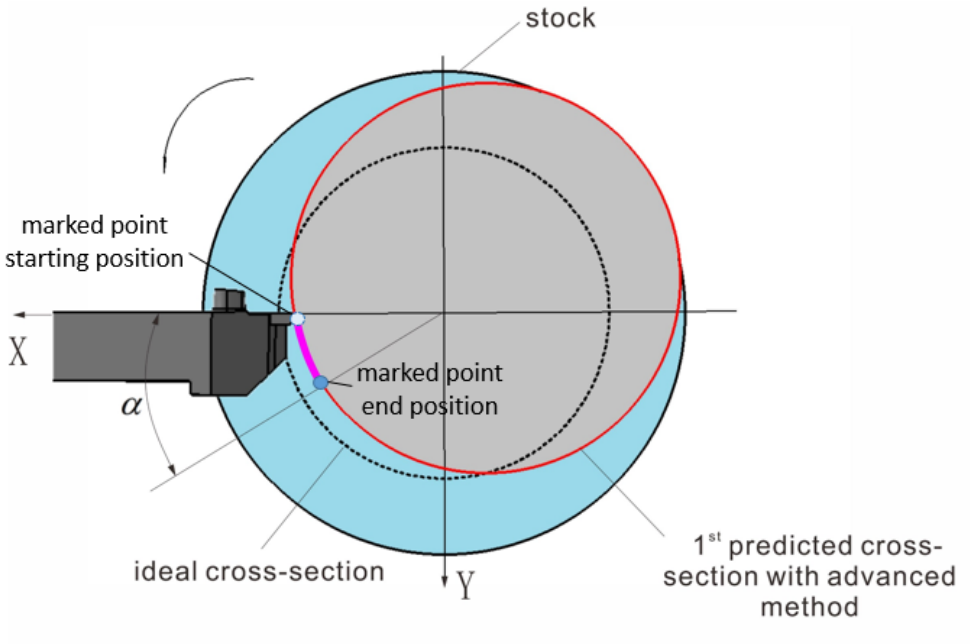

Fig 3.7 The first stage in the first feed per revolution

In the second stage, because of the coupling between the depth of cut and the cutting force, after the depth of cut decreased, and the cutting force then decreased. Then the part is sprung back and the depth of cut increases. The predicted cross-section is then the red circle as shown in Fig 3.8. In this stage, part turns from the end position of the first stage and the blue locus is the trajectory of the first stage. Tracking the position of the contact point that has been marked as the starting point in the first stage, we can now see the part turned 2α deg in total.

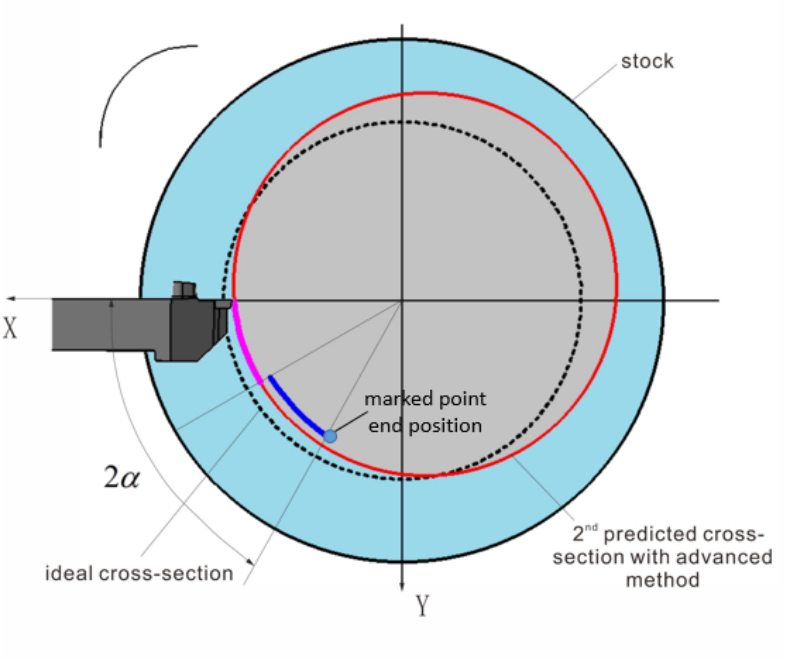

Fig 3.8 The second stage in the first feed per revolution

In the third stage, because of the coupling between the depth of cut and the cutting force, after the change happened in the second stage, the depth of cut becomes smaller as shown in Fig 3.9.

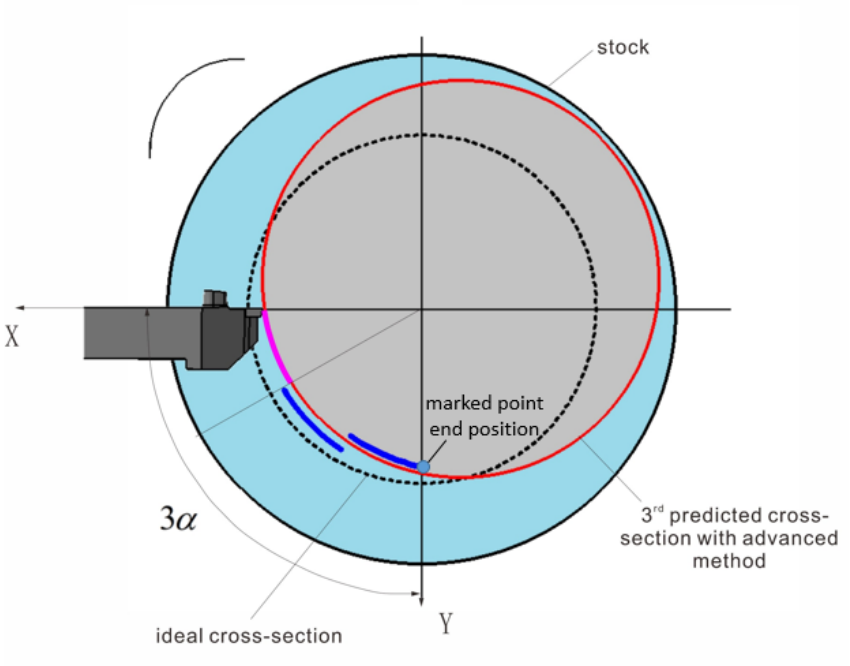

Fig 3.9 The third stage in the first feed per revolution

Following the same logic, the trajectories of the rest of the stages in the first feed per revolution can be obtained. The illustrative result is in Fig 3.10.

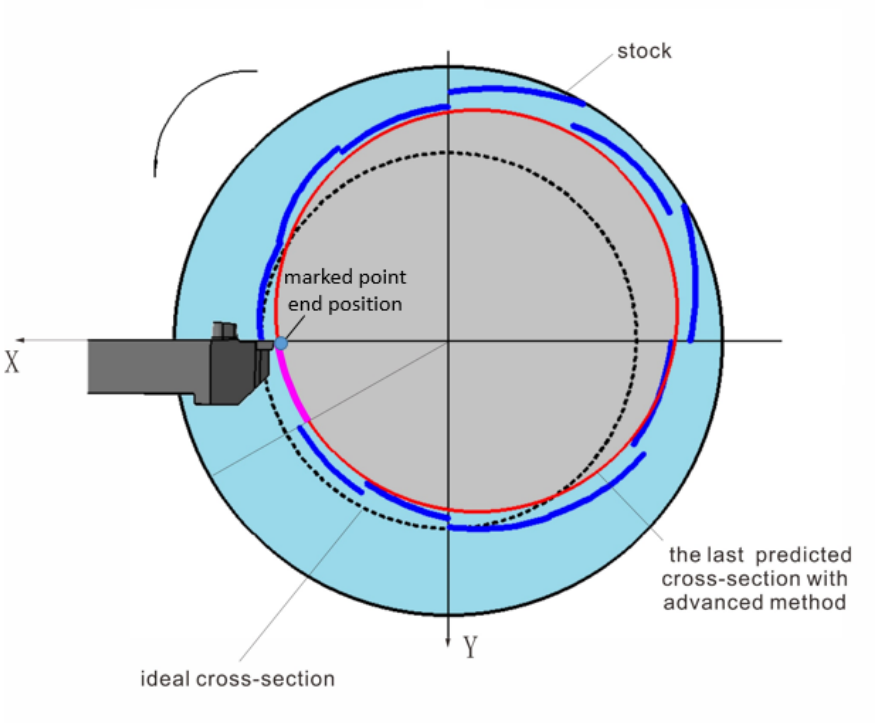

Fig 3.10 The rest of the stages in the first feed per revolution

The diametrical deviation in each stage can be obtained by the finite element model developed in Fig 3.11. The details of the finite element model will be described in the following subsections.

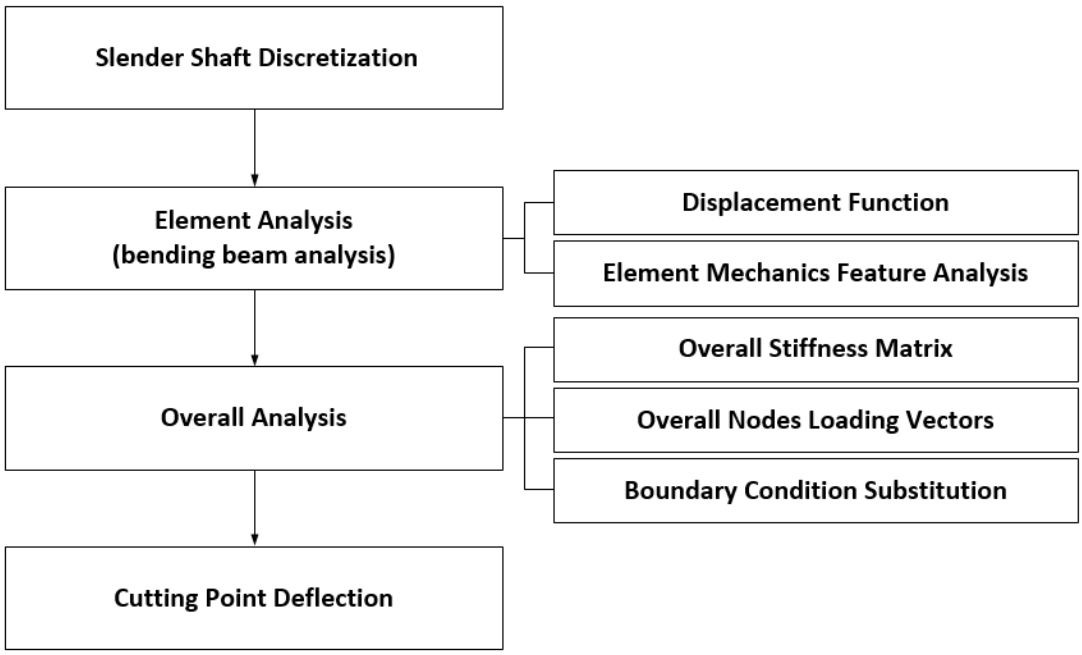

Fig 3.11 The process of finite element analysis

By using the aforementioned algorithm, the diametrical deviation along the first feed per revolution can be yielded. This algorism can be generalized and iterated to obtain the diametrical deviation along the whole slender shaft. The specific model derivation will be constructed in Subsection Chapter 4.

Chapter 4 Derivation of the Discrete and Hybrid Approach

4.1 Geometric analysis in one feed per revolution

Cutting forces are proportional to the un-deformed chip thickness. In turning, the un-deformed chip thickness can be approximated as the product of the depth of cut and the distance that the tool traveled along the feed direction. Since the tool travels along the Z-axis with a uniform speed, the distance the tool travels along the Z-axis is the same within any same period. Thus, the depth

of cut is the main factor influencing the un-deformed chip thickness. As a result, during machining, the cutting force will remain the same, unless the depth of cut changes. In practical situation, the depth of cut changes smoothly due to part deflections created by the push of the tool. However, within a small angle α that the part turns, the depth of cut does not change significantly. Therefore, within this small angle, we can consider the cutting force remaining constant.

In Fig 4.1, α is the angle in which the cutting force does not change and the process that the part turns α is defined as a stage. In one feed per revolution, the part turns 360 degrees, *m* are stages presented in one feed per revolution. m can be derived as:

$$\mathrm{m} = \frac{360^{\circ}}{\alpha}$$

Eq. 4.1

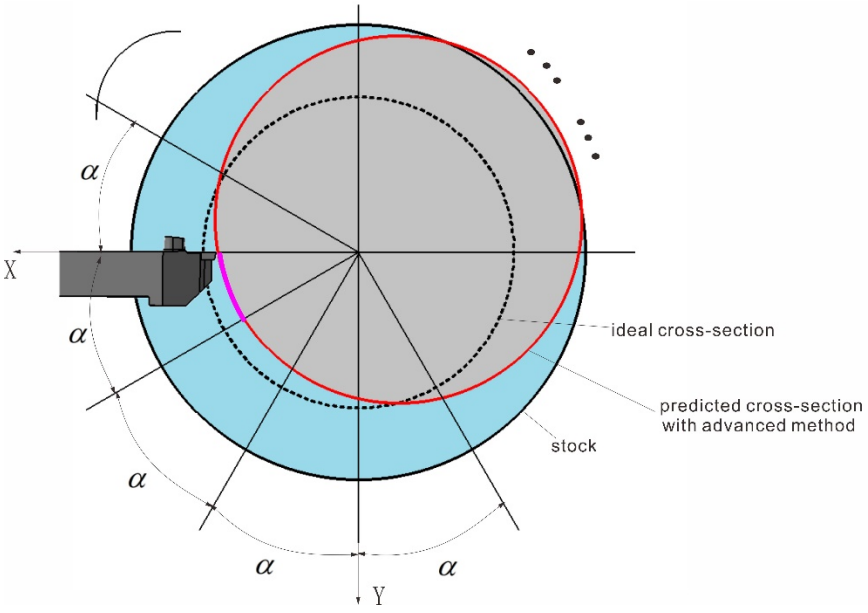

Fig 4.1 Divisions of stages in one feed per revolution

4.2 Prediction of the shaft deflection in one stage

In the actual slender shaft manufacturing, a steady rest is often used to somehow reduce the deflection shaft. Thus, to predict the deflection in one stage, the static equilibrium equations (force and moment equilibrium conditions) are insufficient for determining the internal forces and reactions on the slender shaft. The introduction of the steady rest renders the problem to be a statically indeterminate problem, which the simple mechanics theory cannot solve. Therefore, a finite element method is used to perform the mechanics analysis here.

To develop the finite element model, firstly, two hypotheses are made: 1) the slender shaft is assumed to be an ideal elastomer, meeting the basic assumptions of elasticity mechanics and 2) the cutting force at any instance is assumed to be constant.

The general process of finite element analysis is shown in Fig 3.11. Firstly, the slender shaft will be discretized as a structure consists of elements and nodes. Then, each element will be analyzed. There are two parts of the element analysis: displacement analysis and element mechanics feature analysis. These elements will be assembled together and the boundary conditions will be applied. Subsequently, the overall analysis is performed so that the deflection of the cutting point can be obtained. The overall analysis consists of three parts: overall stiffness matrix, overall nodes loading vectors, and boundary condition substitution.

4.3 Slender shaft discretization

The first step of the finite element method to analyze the slender shaft turning process involves the slender shaft discretization. In this research, nodes are set at where the forces or constraints are applied. Thus, in total four nodes are set respectively at the clamping point of the workpiece on the chuck, at the cutting tool, at the steady rest, and at the tip of the tailstock. These four nodes divide the slender shaft into three pieces. Each of the three pieces is defined as an element in finite element analysis.

Further assumptions are made as the followings. 1) Although in actual situations, the cutting force acting on the workpiece does not only act on one point, and the cutting force varies along the cutting edge. Here we take the cutting force and the position closest to the tool tip in a node. 2) The supporting force of the steady rest on the workpiece does not only act on one point either. But in this finite element model, the centroid of the acting surface between the workpiece and the steady rest is taken as the point where the support force act on another node.

Two possible scenarios are considered during the shaft turning process, namely 1) the tool at the left of the steady rest (see Fig 4.2) and 2) the tool at the right of the steady rest (see Fig 4.3). The special cases where the tool aligns with the tailstock, the steady rest, and the chuck will happen at only three instant moments. Since these special cases will not change the overall deflection of the shaft, they are not discussed here. These two possible cases lead to the node number of each element to be different. However, the finite element analysis of the problem follows the same logic so the analysis on one scenario does not lose generality. The following sections demonstrate the finite element analysis for the scenario where the tool is at the left of the steady rest (see Fig 4.2).

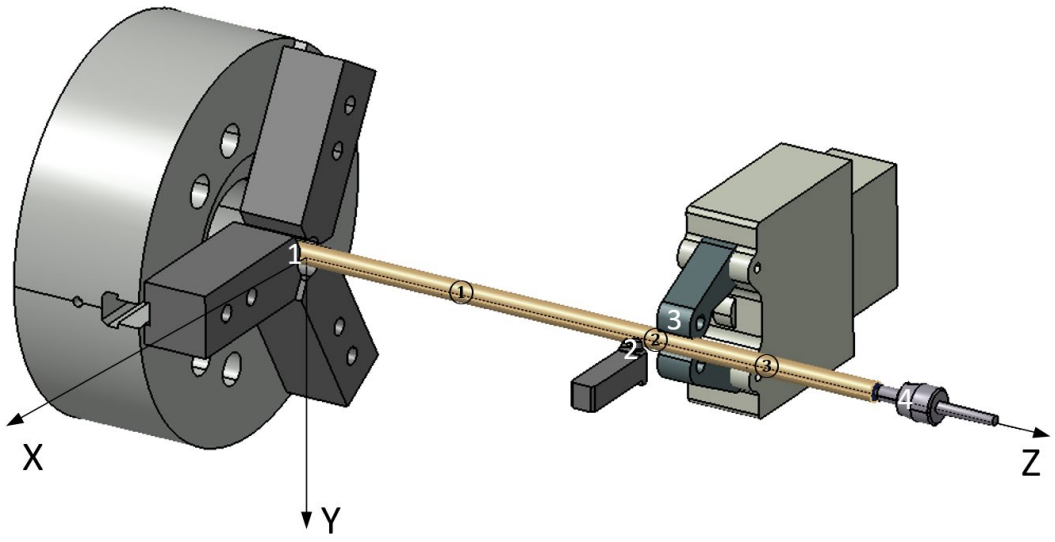

Fig 4.2 The slender shaft discretization (The tool is at the left of the steady rest)

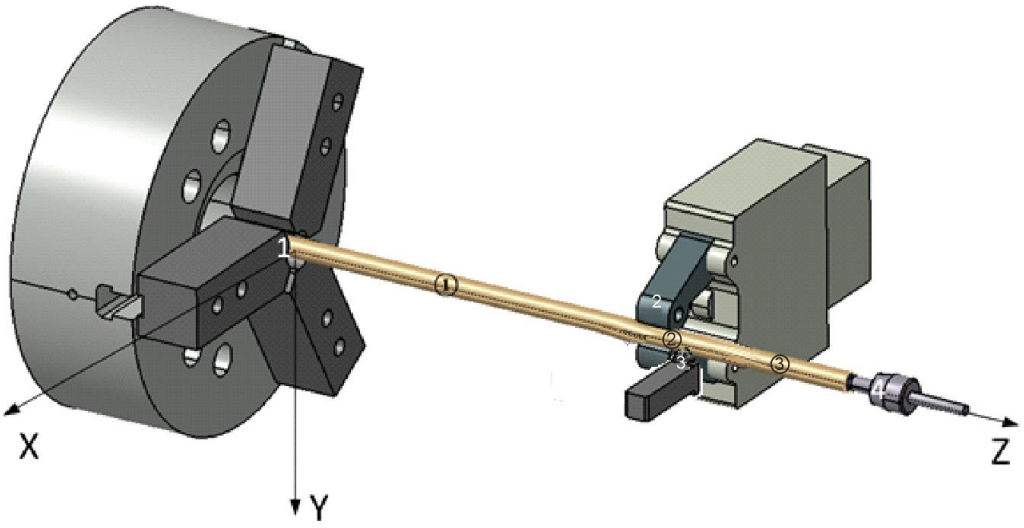

Fig 4.3 The slender shaft discretization (The tool is at the right of the steady rest)

By considering the cutting force acting on node 2 and the supporting force of the steady rest acting on node 3, the slender shaft can be discretized as shown in Fig 4.4. Also, note that the deflections at node 2 in the X and Y direction are u_{wx} and u_{wy} respectively in Eq. 2.3

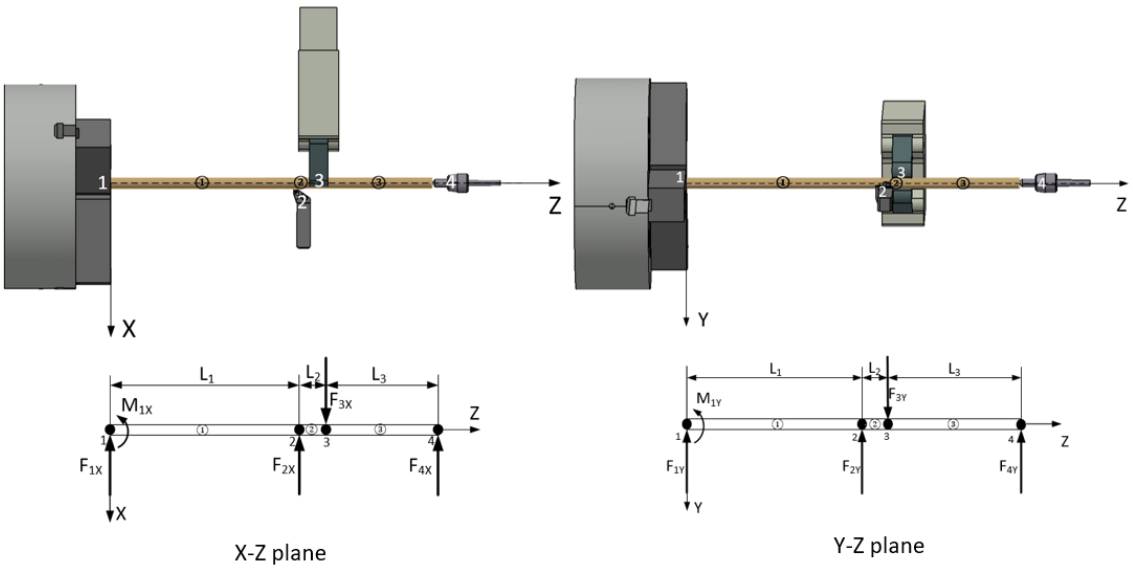

Fig 4.4 The load condition of the discretized slender shaft

4.4 Element analysis

Fig 4.5 is a simple bending beam example, its loading condition is shown below. In the bending beam element analysis, the bottom surface is under tension, so it would become longer along Z-axis. Meanwhile, the top surface is under pressure, so it would become shorter along Z-axis. Between the top surface and the bottom surface, there must exist a layer who keeps the same shape as the original, under neither tension nor pressure. This layer is called the neutral layer.

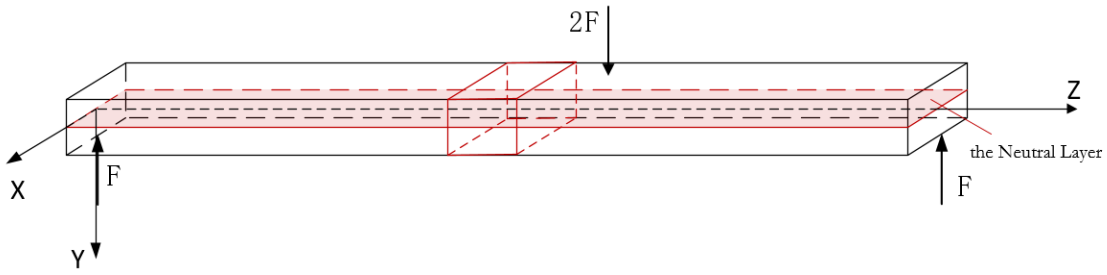

Fig 4.5 Bending element schematic diagram

A micro piece has been taken from Fig 4.5. Fig 4.6 shows this piece from X-direction, in the Y-Z plane. A longitudinal line means a layer and a horizontal line means a cross-section. The neutral layer becomes the neutral curve in this view. Points on the neutral curve are assumed to be displaced vertically only and not horizontally. Cross-sections still remain planes after bending, and orthogonal to the fibers. In bending element analysis, displacement υ means the displacement of the neutral curve and upward is the positive direction. When the internal moment M deforms the element of the beam, the angle between the cross-sections becomes the slope θ as shown in Fig 4.6.

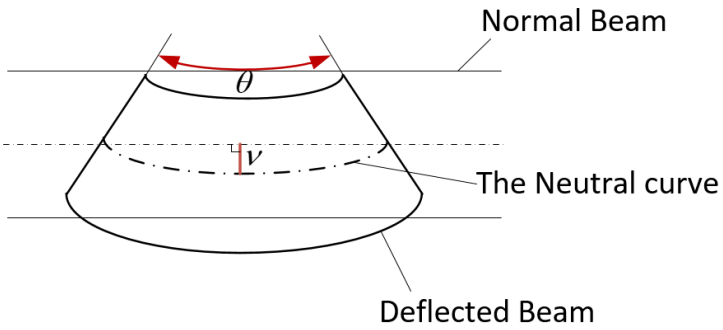

Fig 4.6 Bending element schematic diagram

For each bending beam element, there is a stiffness function, derived from the principle of minimum potential energy, which will be proved later. There are two vectors and one matrix. These two vectors are nodes loading vector P^{e} and nodes displacement vector q^e are defined here,

$$\mathrm{P}^{\mathrm{e}}=\begin{bmatrix}\mathrm{F}_1 & \mathrm{M}_1 & \mathrm{F}_2 & \mathrm{M}_2\end{bmatrix}^{\mathrm{T}}$$

Eq. 4.2

$$q^e=\begin{bmatrix}v_1 & \theta_1 & v_2 & \theta_2\end{bmatrix}^{\mathrm{T}}$$

Eq. 4.3

As shown in Fig 4.7 and Fig 4.8, both ends of the bending beam element are under the influence of shear forces and internal moments, and those shear forces and internal moments consist of nodes loading vectors. The displacements are caused by shear forces and the slopes are caused by the internal moments. They are grouped in the nodes displacement vector. E is the Young's modulus which presents the ability for resisting deformations. I is the moment of inertia of the cross-section which is defined by the shape of the cross-section. l is the length of one of the element beams.

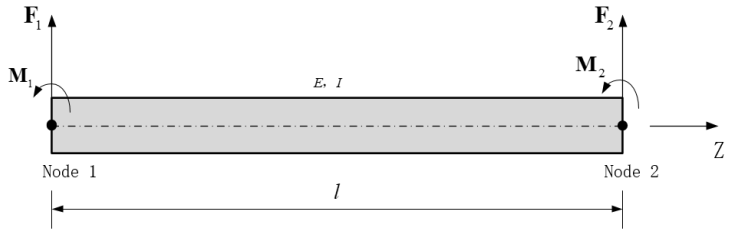

Fig 4.7 Element loading condition

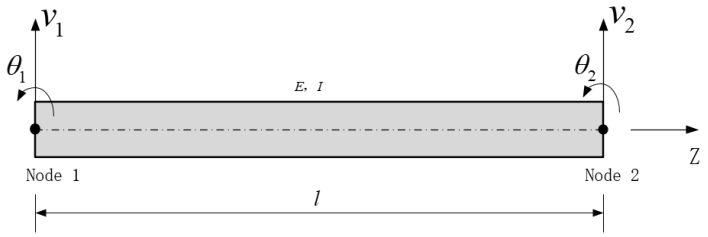

Fig 4.8 Element displacement condition

The Hermite polynomial is used to express the bending beam element in the displacement analysis,

$$v(z) = \left(1-3\xi^2(z)+2\xi^3(z)\right)v_1 + l\left(\xi(z)-2\xi^2(z)+\xi^3(z)\right)\theta_1 + \left(3\xi^2(z)-2\xi^3(z)\right)v_2 + l\left(\xi^3(z)-\xi^2(z)\right)\theta_2$$
$$= N\left(\xi(z)\right)q^e$$

Eq. 4.4

According to the Hermite polynomial (Eq. 4.4), the shape function can be obtained:

$$N\left(\xi(z)\right) = \left[\left(1-3\xi^2(z)+2\xi^3(z)\right) \quad l\left(\xi(z)-2\xi^2(z)+\xi^3(z)\right) \quad \left(3\xi^2(z)-2\xi^3(z)\right) \quad l\left(\xi^3(z)-\xi^2(z)\right)\right]$$

Eq. 4.5

where

$$\xi = \frac{x}{l}$$

Eq. 4.6

In the mechanics analysis for statics, three aspects are involved: strain, stress, and displacement. The finite element analysis is the same. It uses forms of vectors and matrix to express these three aspects, in order to build a mechanics function. This function is known as the stiffness function. In this section, how strain, stress, and displacement are expressed in finite element analysis will be introduced.

As shown in Fig 4.9 *Micro-piece in bending beam element*, the filled part is a micro piece taken from the bending beam. It is called an element. As the neutral curve is a curve in the cross-

section of a beam or a shaft along which there is no longitudinal stress or strain. So the length of the neutral curve is the original length of this micro-piece. y is defined as the coordinate value along the radius direction in Fig 4.9 *Micro-piece in bending beam element*. The neutral curve is defined as y_0. The other layers with deformed length have a distance y to the neutral curve is shown below. $d\theta$ is the slope of this micro-piece. R is the radius of the curvature of this micro-piece.

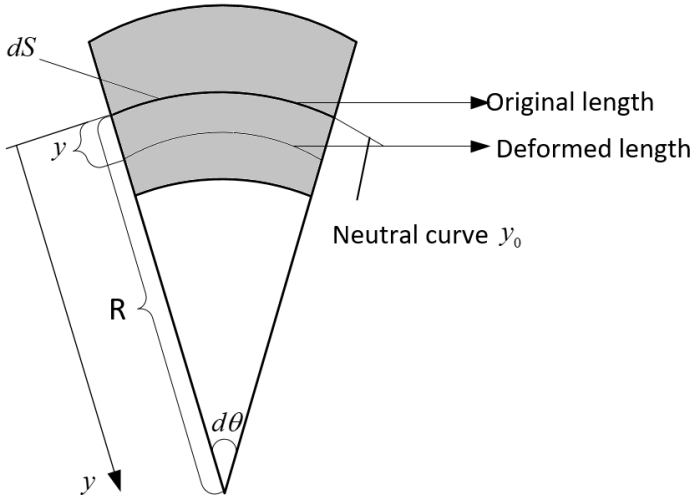

Fig 4.9 Micro-piece in bending beam element

According to geometric principles of the deformed bending beam element, the strain of the layer located on y is obtained:

$$\varepsilon(y) = \frac{(R-y)\cdot d\theta - R\cdot d\theta}{R\cdot d\theta} = -\frac{y}{R}$$

Eq. 4.7

Combined with the relationship between curvature K and the radius of curvature R:

$$K = \frac{d\theta}{ds} = \frac{d\theta}{R\cdot d\theta} = \frac{1}{R}$$

Eq. 4.8

According to the theories in calculus [24], the curvature of a point on a plane is:

$$K = \frac{v''(z, y_0)}{\left(1 + v'(z, y_0)^2\right)^{\frac{3}{2}}} \approx v''(z, y_0)$$

Eq. 4.9

Because in elasticity mechanics, the deformation of a solid body is assumed to be infinitely small, we have

$$K = \frac{\mathrm{d}^2 v(z, y_0)}{dx^2}$$

Eq. 4.10

Therefore, the geometric function is obtained:

$$\varepsilon(z, y_0) = -y \frac{d^2 v(z, y_0)}{dz^2}$$

Eq. 4.11

The geometric matrix is defined as:

$$B(\xi) = -y \begin{bmatrix} B_1 & B_2 & B_3 & B_4 \end{bmatrix}$$

Eq. 4.12

The geometric function aims to show the relationship between the strain $\varepsilon(z, y_0)$ and the displacement q^e. So the geometric matrix is substituted into the geometric function:

$$\varepsilon(z, y_0) = -y \frac{d^2 v(z)}{dz^2} = -y \left[\frac{1}{l^2}(12\xi(z) - 6) \quad \frac{1}{l}(6\xi(z) - 4) \quad -\frac{1}{l^2}(12\xi(z) - 6) \quad \frac{1}{l}(6\xi(z) - 4) \right] q^e = B(\xi) q^e$$

Eq. 4.13

The stress analysis aims to show the relationship between the strain and the stress. According to Hooke's law, the stress function of a layer in the bending beam element is:

$$\sigma(z, y_0) = EB(\xi) q^e$$

Eq. 4.14

As the displacement function has been explained as the shape function (Eq. 4.5), the stiffness function consists of strain, stress, and displacement could be obtained.

The element strain energy is:

$$U^{\mathrm{e}} = \frac{1}{2}\int_0^l \int_A \sigma(z,y)\varepsilon(z,y)\,dA dx = \frac{1}{2} q^{e^{\mathrm{T}}} \left[\int_0^l \int_A B^{\mathrm{T}}(\xi) EB(\xi)\,dA dx \right] = \frac{1}{2} q^{e^T} \mathrm{K}^e q^e$$

Eq. 4.15

where,

$$\mathrm{K}^e = \int_0^l \int_A (-y) \begin{bmatrix} B_1 \\ B_2 \\ B_3 \\ B_4 \end{bmatrix} E \begin{bmatrix} B_1 & B_2 & B_3 & B_4 \end{bmatrix} (-y)\,dA dx$$

$$= \int_A (-y)^2 dA E \int_0^l \begin{bmatrix} B_1{}^2 & B_1B_2 & B_1B_3 & B_1B_4 \\ B_1B_2 & B_2{}^2 & B_2B_3 & B_2B_4 \\ B_1B_3 & B_2B_3 & B_3{}^2 & B_3B_4 \\ B_1B_4 & B_2B_4 & B_3B_4 & B_4{}^2 \end{bmatrix} dz = \frac{EI}{l^3} \begin{bmatrix} 12 & 6l & -12 & 6l \\ 6l & 4l^2 & -6l & 2l^2 \\ -12 & -6l & 12 & -6l \\ 6l & 2l^2 & -6l & 4l^2 \end{bmatrix}$$

Eq. 4.16

And the work of the external forces is:

$$W^{\mathrm{e}} = \mathrm{F}_1 \nu_1 + \mathrm{M}_1 \theta_1 + \mathrm{F}_2 \nu_2 + \mathrm{M}_2 \theta_2 = \mathrm{P}^e q^e$$

Eq. 4.17

where, P^e is the nodes loading vector.

According to the minimum total potential energy principle, the total energy is:

$$\Pi(q^e) = U^e - W^e = \frac{1}{2} q^{\mathrm{eT}} \cdot \mathrm{K}^e \cdot q^e - \mathrm{P}^{\mathrm{eT}} \cdot q^e$$

Eq. 4.18

The condition for the total energy to be minimum is

$$\frac{\partial \Pi(q^e)}{\partial (q^e)} = 0$$

Eq. 4.19

From to *Eq. 4.18* and *Eq. 4.19*, we have

$$\mathrm{K}^{\mathrm{e}} \cdot q^e = \mathrm{P}^{\mathrm{e}}$$

Eq. 4.20

Eq.3.20 is the element stiffness function that is needed in the following derivation.

4.5 The overall analysis of the bending slender shaft

The physical meaning of the element stiffness matrix K^{e} is the element ability to resist deformation. Each item in the element stiffness matrix means how much force or torque will be needed to cause the unit displacement. It has the same physical nature as the coefficient of elasticity of the spring.

Therefore, as shown in *Fig 3.2*, the slender shaft consists of three bending beam elements connected by nodes. The overall stiffness matrix K of the slender shaft can be written as:

$$K=\begin{bmatrix}
\frac{12EI_1}{L_1^3} & \frac{6EI_1}{L_1^2} & -\frac{12EI_1}{L_1^3} & \frac{6EI_1}{L_1^2} & 0 & 0 & 0 & 0 \\
\frac{6EI_1}{L_1^2} & \frac{4EI_1}{L_1} & -\frac{6EI_1}{L_1^2} & \frac{2EI_1}{L_1} & 0 & 0 & 0 & 0 \\
-\frac{12EI_1}{L_1^3} & -\frac{6EI_1}{L_1^2} & \frac{12EI_1}{L_1^3}+\frac{12EI_2}{L_2^3} & -\frac{6EI_1}{L_1^2}+\frac{6EI_2}{L_2^2} & -\frac{12EI_2}{L_2^3} & \frac{6EI_2}{L_2^2} & 0 & 0 \\
\frac{6EI_1}{L_1^2} & \frac{2EI_1}{L_1} & -\frac{6EI_1}{L_1^2}+\frac{6EI_2}{L_2^2} & \frac{4EI_1}{L_1}+\frac{4EI_2}{L_2} & -\frac{6EI_2}{L_2^2} & \frac{2EI_2}{L_2} & 0 & 0 \\
0 & 0 & -\frac{12EI_2}{L_2^3} & -\frac{6EI_2}{L_2^2} & \frac{12EI_2}{L_2^3}+\frac{12EI_3}{L_3^3} & -\frac{6EI_2}{L_2^2}+\frac{6EI_3}{L_3^2} & -\frac{12EI_3}{L_3^3} & \frac{6EI_3}{L_3^2} \\
0 & 0 & \frac{6EI_2}{L_2^2} & \frac{2EI_2}{L_2} & -\frac{6EI_2}{L_2^2}+\frac{6EI_3}{L_3^2} & \frac{4EI_2}{L_2}+\frac{4EI_3}{L_3} & -\frac{6EI_3}{L_3^2} & \frac{2EI_3}{L_3} \\
0 & 0 & 0 & 0 & -\frac{12EI_3}{L_3^3} & -\frac{6EI_3}{L_3^2} & \frac{12EI_3}{L_3^3} & -\frac{6EI_3}{L_3^2} \\
0 & 0 & 0 & 0 & \frac{6EI_3}{L_3^2} & \frac{2EI_3}{L_3} & -\frac{6EI_3}{L_3^2} & \frac{4EI_3}{L_3}
\end{bmatrix}$$

Eq. 4.21

Then the overall stiffness function in the X and Y direction can be obtained:

$$\begin{bmatrix}
\frac{12EI_1}{L_1^3} & \frac{6EI_1}{L_1^2} & -\frac{12EI_1}{L_1^3} & \frac{6EI_1}{L_1^2} & 0 & 0 & 0 & 0 \\
\frac{6EI_1}{L_1^2} & \frac{4EI_1}{L_1} & -\frac{6EI_1}{L_1^2} & \frac{2EI_1}{L_1} & 0 & 0 & 0 & 0 \\
-\frac{12EI_1}{L_1^3} & -\frac{6EI_1}{L_1^2} & \frac{12EI_1}{L_1^3}+\frac{12EI_2}{L_2^3} & -\frac{6EI_1}{L_1^2}+\frac{6EI_2}{L_2^2} & -\frac{12EI_2}{L_2^3} & \frac{6EI_2}{L_2^2} & 0 & 0 \\
\frac{6EI_1}{L_1^2} & \frac{2EI_1}{L_1} & -\frac{6EI_1}{L_1^2}+\frac{6EI_2}{L_2^2} & \frac{4EI_1}{L_1}+\frac{4EI_2}{L_2} & -\frac{6EI_2}{L_2^2} & \frac{2EI_2}{L_2} & 0 & 0 \\
0 & 0 & -\frac{12EI_2}{L_2^3} & -\frac{6EI_2}{L_2^2} & \frac{12EI_2}{L_2^3}+\frac{12EI_3}{L_3^3} & -\frac{6EI_2}{L_2^2}+\frac{6EI_3}{L_3^2} & -\frac{12EI_3}{L_3^3} & \frac{6EI_3}{L_3^2} \\
0 & 0 & \frac{6EI_2}{L_2^2} & \frac{2EI_2}{L_2} & -\frac{6EI_2}{L_2^2}+\frac{6EI_3}{L_3^2} & \frac{4EI_2}{L_2}+\frac{4EI_3}{L_3} & -\frac{6EI_3}{L_3^2} & \frac{2EI_3}{L_3} \\
0 & 0 & 0 & 0 & -\frac{12EI_3}{L_3^3} & -\frac{6EI_3}{L_3^2} & \frac{12EI_3}{L_3^3} & -\frac{6EI_3}{L_3^2} \\
0 & 0 & 0 & 0 & \frac{6EI_3}{L_3^2} & \frac{2EI_3}{L_3} & -\frac{6EI_3}{L_3^2} & \frac{4EI_3}{L_3}
\end{bmatrix}
\begin{bmatrix} v_{1x} \\ \theta_{1x} \\ v_{2x} \\ \theta_{2x} \\ v_{3x} \\ \theta_{3x} \\ v_{4x} \\ \theta_{4x} \end{bmatrix}
=
\begin{bmatrix} F_{1x} \\ M_{1x} \\ F_{2x} \\ M_{2x} \\ F_{3x} \\ M_{3x} \\ F_{4x} \\ M_{4x} \end{bmatrix}$$

Eq. 4.22

$$\begin{bmatrix} \frac{12EI_1}{L_1^3} & \frac{6EI_1}{L_1^2} & -\frac{12EI_1}{L_1^3} & \frac{6EI_1}{L_1^2} & 0 & 0 & 0 & 0 \\ \frac{6EI_1}{L_1^2} & \frac{4EI_1}{L_1} & -\frac{6EI_1}{L_1^2} & \frac{2EI_1}{L_1} & 0 & 0 & 0 & 0 \\ -\frac{12EI_1}{L_1^3} & -\frac{6EI_1}{L_1^2} & \frac{12EI_1}{L_1^3}+\frac{12EI_2}{L_2^3} & -\frac{6EI_1}{L_1^2}+\frac{6EI_2}{L_2^2} & -\frac{12EI_2}{L_2^3} & \frac{6EI_2}{L_2^2} & 0 & 0 \\ \frac{6EI_1}{L_1^2} & \frac{2EI_1}{L_1} & -\frac{6EI_1}{L_1^2}+\frac{6EI_2}{L_2^2} & \frac{4EI_1}{L_1}+\frac{4EI_2}{L_2} & -\frac{6EI_2}{L_2^2} & \frac{2EI_2}{L_2} & 0 & 0 \\ 0 & 0 & -\frac{12EI_2}{L_2^3} & -\frac{6EI_2}{L_2^2} & \frac{12EI_2}{L_2^3}+\frac{12EI_3}{L_3^3} & -\frac{6EI_2}{L_2^2}+\frac{6EI_3}{L_3^2} & -\frac{12EI_3}{L_3^3} & \frac{6EI_3}{L_3^2} \\ 0 & 0 & \frac{6EI_2}{L_2^2} & \frac{2EI_2}{L_2} & -\frac{6EI_2}{L_2^2}+\frac{6EI_3}{L_3^2} & \frac{4EI_2}{L_2}+\frac{4EI_3}{L_3} & -\frac{6EI_3}{L_3^2} & \frac{2EI_3}{L_3} \\ 0 & 0 & 0 & 0 & -\frac{12EI_3}{L_3^3} & -\frac{6EI_3}{L_3^2} & \frac{12EI_3}{L_3^3} & -\frac{6EI_3}{L_3^2} \\ 0 & 0 & 0 & 0 & \frac{6EI_3}{L_3^2} & \frac{2EI_3}{L_3} & -\frac{6EI_3}{L_3^2} & \frac{4EI_3}{L_3} \end{bmatrix} \begin{bmatrix} v_{1y} \\ \theta_{1y} \\ v_{2y} \\ \theta_{2y} \\ v_{3y} \\ \theta_{3y} \\ v_{4y} \\ \theta_{4y} \end{bmatrix} = \begin{bmatrix} F_{1y} \\ M_{1y} \\ F_{2y} \\ M_{2y} \\ F_{3y} \\ M_{3y} \\ F_{4y} \\ M_{4y} \end{bmatrix}$$

Eq. 4.23

4.6 Solution for the finite element model for predicting the diametrical deviation

To solve the finite element model, loading conditions, boundary conditions, and initial conditions must be applied to the model. Specifically, cutting force components and other constraints must be substituted into the stiffness function above. This is the major difficulty in the prediction of diameter error in slender shaft turning because of the coupling between the depth of cut and the cutting force. In traditional methods, before the turning process begins, the optimized depth of cut and the cutting force can be obtained by an iterative optimization algorithm. However, in the real situation, because the position of the cutting tool keeps changing, the stiffness matrix above keeps changing. Thus, the depth of cut and the cutting force in every moment during the turning process is different. The traditional method did not consider these situations. The cutting force substituted in this novel model which fits the real situation is given as follows.

In Chapter 2, the geometric analysis proves that u_{wx} and u_{wy} are functions of the cutting force components F_r and F_t. The cutting force components F_r and F_t need to be known accurately to calculate the diameter error in slender shaft turning. Based on the cutting force model proposed

in [21], this model was claimed by the author that can be applicable in many sorts of machining, including turning. According to [22] and [23], α_r is the normal rake angle and it is influenced by the back rake α_b , side rake α_s , and lead angle γ_L of the cutter. λ is the inclination angle. A_c is the uncut chip area. f is the feed rate. d_n is the nominal cutting depth.

$$F_t = -K_n A_c[\cos\alpha_b \cos\gamma_{Le} + K_f(\cos\gamma_{Le} \sin\alpha_r + \sin\gamma_{Le} \sin\alpha_b)]$$

Eq. 4.24

$$F_r = -K_n A_c[-\sin\alpha_b + K_r \sin\gamma_{Le} \cos\alpha_b]$$

Eq. 4.25

$$F_a = K_n A_c[-\cos\alpha_b \sin\alpha_r + K_f(\cos\gamma_{Le} \cos\alpha_r)]$$

Eq. 4.26

where,

$$A_c = fd_n$$

Eq. 4.27

$$\alpha_r = \arctan[\cos\lambda(\tan\alpha_s \cos\gamma_L + \tan\alpha_b \sin\gamma_L)]$$

Eq. 4.28

where,

$$\lambda = \arctan(\tan\alpha_b \cos\gamma_L - \tan\alpha_s \sin\gamma_L)$$

Eq. 4.29

In the above equations, K_n is the normal cutting pressure. K_f is effective friction coefficient. They are both empirically determined. The calculation of the effective lead angle γ_{Le} is introduced in [23].

The loading conditions can be described as follows. In slender shaft turning with the steady rest, as shown in Fig 4.2, F_{1x}, M_{1x}, F_{1y}, M_{1y} are caused by the chuck. They are unknowns. F_{2x}, M_{2x},

F_{2y}, M_{2y} are caused by the cutting tool. F_{2x}, F_{2y} are cutting force and M_{2x}, M_{2y} are zero. F_{3x}, M_{3x}, F_{3y}, M_{3y} are caused by the steady rest. F_{3x}, F_{3y} are the support forces which are unknowns. Both M_{3x}, M_{3y} are zero. F_{4x}, M_{4x}, F_{4y}, M_{4y} are caused by the tailstock. F_{4x}, F_{4y} are the supporting force of the tailstock and they are unknowns. Both M_{4x}, M_{4y} are zero. Then the overall loading vector in the X and Y directions becomes:

$$\begin{bmatrix} F_{1x} \\ M_{1x} \\ F_{2x} \\ M_{2x} \\ F_{3x} \\ M_{3x} \\ F_{4x} \\ M_{4x} \end{bmatrix} = \begin{bmatrix} F_{1x} \\ M_{1x} \\ F_{fx} \\ 0 \\ F_{r} \\ 0 \\ F_{4x} \\ 0 \end{bmatrix}$$

Eq. 4.30

$$\begin{bmatrix} F_{1y} \\ M_{1y} \\ F_{2y} \\ M_{2y} \\ F_{3y} \\ M_{3y} \\ F_{4y} \\ M_{4y} \end{bmatrix} = \begin{bmatrix} F_{1y} \\ M_{1y} \\ F_{fy} \\ 0 \\ F_{t} \\ 0 \\ F_{4y} \\ 0 \end{bmatrix}$$

Eq. 4.31

The boundary conditions are stated as follows. The chuck, the tailstock, and the steady rest are used to limit the displacement of the slender shaft in the turning process. Thus, the displacements $v_{1x}, \theta_{1x}, v_{1y}, \theta_{1y}$ are zero due to the limit of the chuck. The displacements v_{3x}, v_{3y} are zero due to the limit of the steady rest. The displacements v_{4x}, v_{4y} are zero due to the limit of the

tailstock. From the boundary conditions above, the overall displacement vector in the X and Y direction becomes:

$$\begin{bmatrix} \nu_{1x} \\ \theta_{1x} \\ \nu_{2x} \\ \theta_{2x} \\ \nu_{3x} \\ \theta_{3x} \\ \nu_{4x} \\ \theta_{4x} \end{bmatrix} = \begin{bmatrix} 0 \\ 0 \\ \nu_{2x} \\ \theta_{2x} \\ 0 \\ \theta_{3x} \\ 0 \\ \theta_{4x} \end{bmatrix}$$

Eq. 4.32

$$\begin{bmatrix} \nu_{1y} \\ \theta_{1y} \\ \nu_{2y} \\ \theta_{2y} \\ \nu_{3y} \\ \theta_{3y} \\ \nu_{4y} \\ \theta_{4y} \end{bmatrix} = \begin{bmatrix} 0 \\ 0 \\ \nu_{2y} \\ \theta_{2y} \\ 0 \\ \theta_{3y} \\ 0 \\ \theta_{4y} \end{bmatrix}$$

Eq. 4.33

ν_{2x}, ν_{2y} are the deflections caused by cutting forces. They equal to u_{wx}, u_{wy} defined in Chapter 2, respectively. The overall stiffness matrix K is depending on the physical properties of the slender shaft, which is known in real manufacturing. The overall loading vector can be calculated based on the principles of metal cutting. All the unknown parts could be eliminated according to the characteristics of the partitioned matrix. Therefore, the overall displacement vector can be obtained, meaning that ν_{2x}, ν_{2y} (u_{wx}, u_{wy}) can be obtained,

$$\nu = K^{-1} F$$

Eq. 4.34

4.7 The prediction of the diametrical deviation in the first feed per revolution

As shown in Fig 4.10, a slender shaft is being machined. L is the length of the slender shaft. f is the feed rate. At this moment, the tool is at the position Z_t along the Z-axis and the tool locates on the right to the steady rest and the location of the steady rest is Z_r. Referring to Fig 4.3, the length of the first element (from the chuck to the steady rest), is L_1 and

$$L_1 = Z_s$$

Eq. 4.35

The length of the second element (from the steady rest to the cutting tool) is L_2 and

$$L_2 = Z_t - L_1$$

Eq. 4.36

The length of the third element (the length from the cutting tool to the tailstock) is L_3 and

$$L_3 = L - Z_t$$

Eq. 4.37

Since the position of the tool along the shaft axis changes during machining. Z_t will change accordingly, resulting in the length L_2 and L_3 to change.

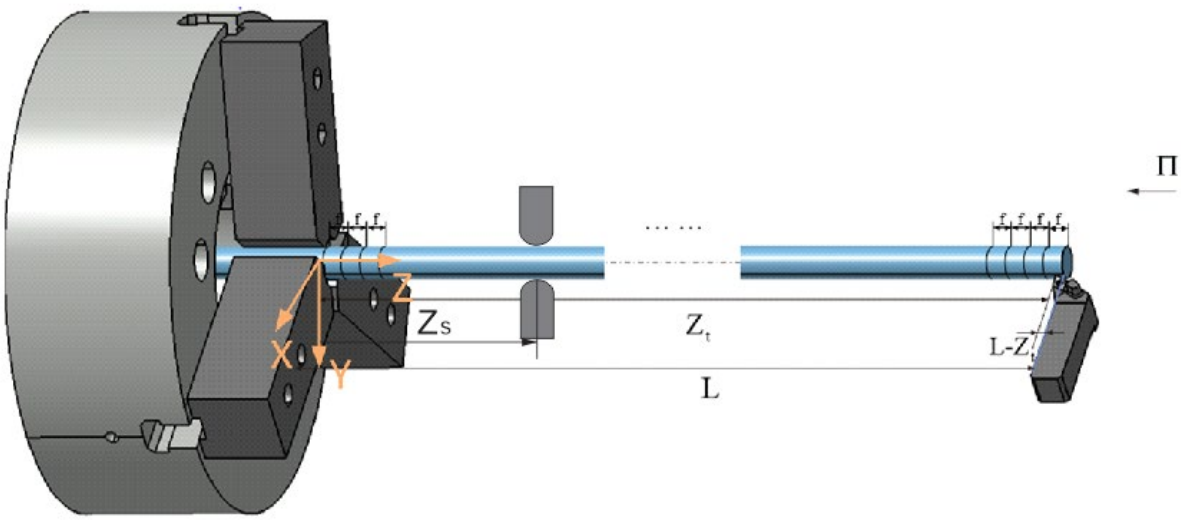

Fig 4.10 The complete turning process of the slender shaft

The analysis starts from the first feed per revolution. In the first stage in the first feed per revolution, the part turns α as shown below. a_1 is the depth of cut in the first stage. D is the diameter of the stock. R_1 is the radius of the first predicted cross-section with the novel method.

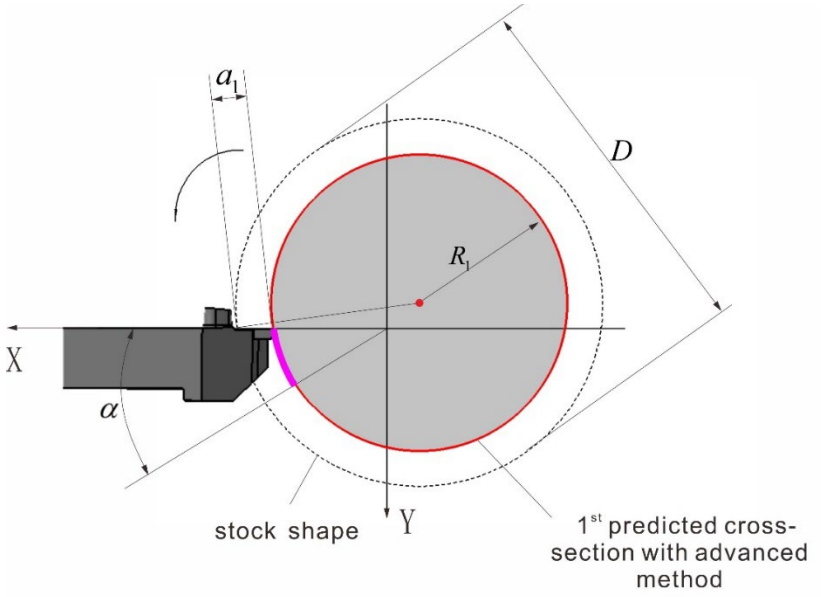

Fig 4.11 The first stage in the first feed per revolution

The initial condition considers that the initial depth of cut is the nominal depth of cut and the cutting forces components are obtained from Eq. 4.24 to Eq. 4.29 using the initial depth of cut.

$$F_{t1} = F_t(a_1)$$

Eq. 4.38

$$F_{r1} = F_r(a_1)$$

Eq. 4.39

Since only a small amount of change occurs with the moment of inertia I, the moment of inertia is set to be constant and it is found by using the nominal diameter of the stock. Also, the Young's modulus (E) is the characteristics of the shaft, it will be a constant.

With the parameters including the lengths between the chuck and the steady rest (L_1), the steady rest and the tool (L_2), the tool and the center (L_3), the tangential cutting force component (F_t), the radial cutting force component (F_r), the Young's modulus (E), the moment of inertia (I), the nominal depth of cut (d_n), we can find the diametrical deviation of the shaft in this stage using Eq. 4.34 and Eq. 2.5. Here, we define a function $g(F_t, F_r, Z_t, Z_s)$ to represent the diametrical deviation and the function g includes the FEA model described in subsections 3.4.3 to 3.4.6.

From Fig 4.10, in each stage within any feed per revolution, the Z coordinate of the tool can be calculated as

$$Z_t = (i - 1 + \frac{k \cdot \alpha}{360}) \cdot f$$

Eq. 4.40

where i is the ordinal of feed per revolution and k is the ordinal of the stage in i feed per revolution. The radial deviation δ_1 of the first stage in the first feed per revolution can be written as a function as shown below:

$$\delta_1 = \mathrm{g}(\mathrm{F_{t1}}, \mathrm{F_{r1}}, \mathrm{Z_{t1}}, \mathrm{Z_s})$$

Eq. 4.41

where,

$$\mathrm{Z_{t1}} = (0 + \frac{\alpha}{360}) \cdot f$$

Eq. 4.42

$\mathrm{Z_s}$ is a value set according to the actual manufacturing situation. The radius of the cross-section at the end of the first stage can be written as:

$$R_1 = \frac{D}{2} - \delta_1$$

Eq. 4.43

The second stage in the first feed per revolution is shown in Fig 4.12 and $\mathrm{a_2}$ is the depth of cut, it is obtained as:

$$\mathrm{a_2} = \frac{D}{2} - R_1$$

Eq. 4.44

where R_1 is the radius of the first stage, D is the diameter of the stock. The cutting force components in the second stage is shown below:

$$F_{t2} = F_t(\mathrm{a_2})$$

Eq. 4.45

$$F_{r2} = F_r(a_2)$$

Eq. 4.46

The radial deviation in the second stage can be written as:

$$\delta_2 = g(F_{t2}, F_{r2}, Z_{t2}, Z_s)$$

Eq. 4.47

where,

$$Z_{t2} = (0 + \frac{2\alpha}{360}) \cdot f$$

Eq. 4.48

The radius of the cross-section at the end of the second stage can be written as:

$$R_2 = \frac{D}{2} - \delta_2$$

Eq. 4.49

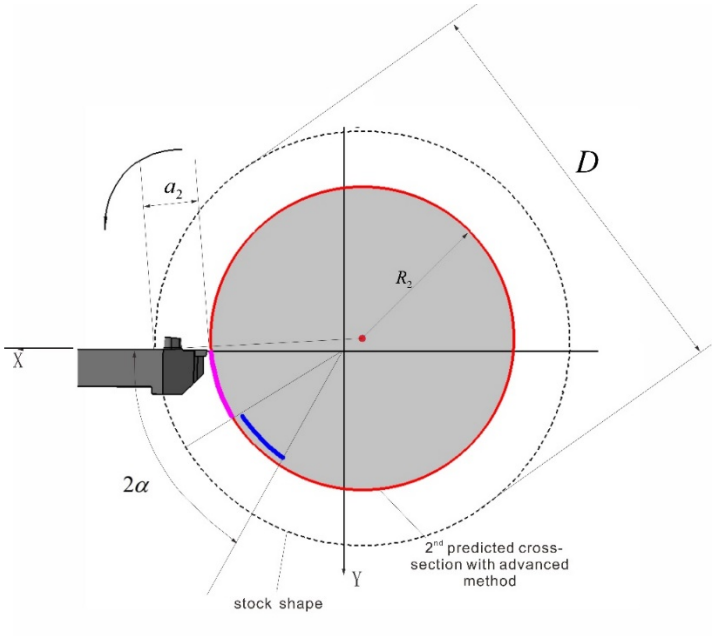

Fig 4.12 The second stage in the first feed per revolution

For the third stage of the first feed per revolution as shown in Fig 4.13 and a_3 is the depth of cut. It is obtained as:

$$a_3 = \frac{D}{2} - R_2$$

Eq. 4.50

The cutting force components in the third stage is shown below:

$$F_{t3} = F_t(a_3)$$

Eq. 4.51

$$F_{r3} = F_r(a_3)$$

Eq. 4.52

The radial deviation in the third stage can be written as:

$$\delta_3 = g(F_{t3}, F_{r3}, Z_{t3}, Z_s)$$

Eq. 4.53

where,

$$Z_{t3} = (0 + \frac{3\alpha}{360}) \cdot f$$

Eq. 4.54

The radius of the cross-section at the end of the second stage can be written as:

$$R_3 = \frac{D}{2} - \delta_3$$

Eq. 4.55

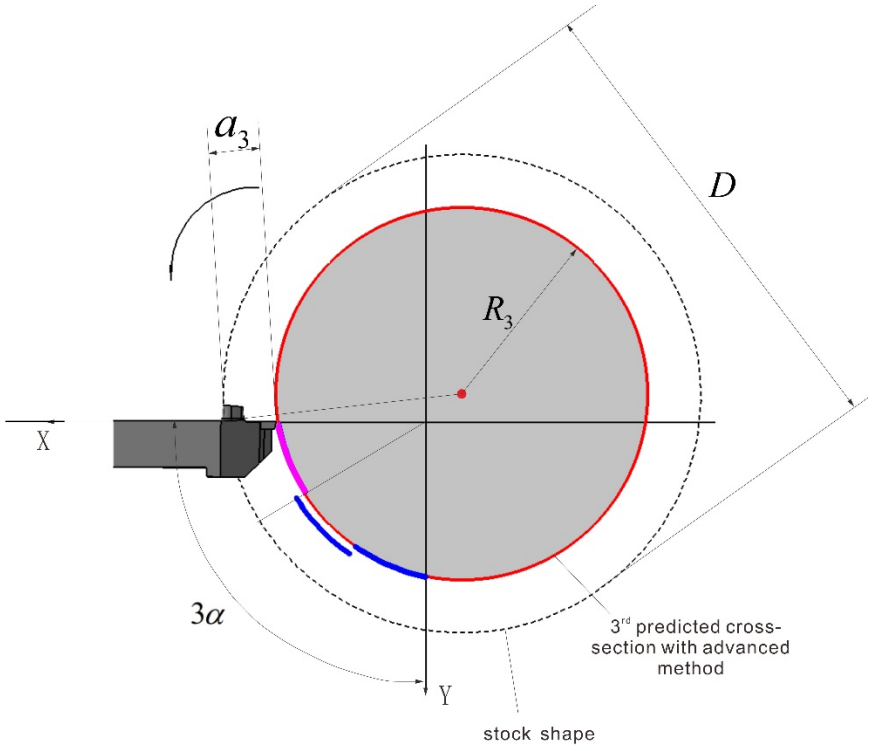

Fig 4.13 The third stage in the first feed per revolution

For the last stage of the first feed per revolution as shown in Fig 4.14, a_m is the depth of cut, it is obtained as:

$$a_m = \frac{D}{2} - R_{m-1}$$

Eq. 4.56

The cutting force components in the third stage is shown below:

$$F_{tm} = F_t(a_m)$$

Eq. 4.57

$$F_{rm} = F_r(a_m)$$

Eq. 4.58

The radial deviation in the third stage can be written as:

$$\delta_m = g(F_{tm}, F_{rm}, Z_{tm}, Z_s)$$

Eq. 4.59

where,

$$Z_{tm} = (0 + \frac{m\alpha}{360}) \cdot f$$

Eq. 4.60

The radius of the cross-section at the end of the second stage can be written as:

$$R_m = \frac{D}{2} - \delta_m$$

Eq. 4.61

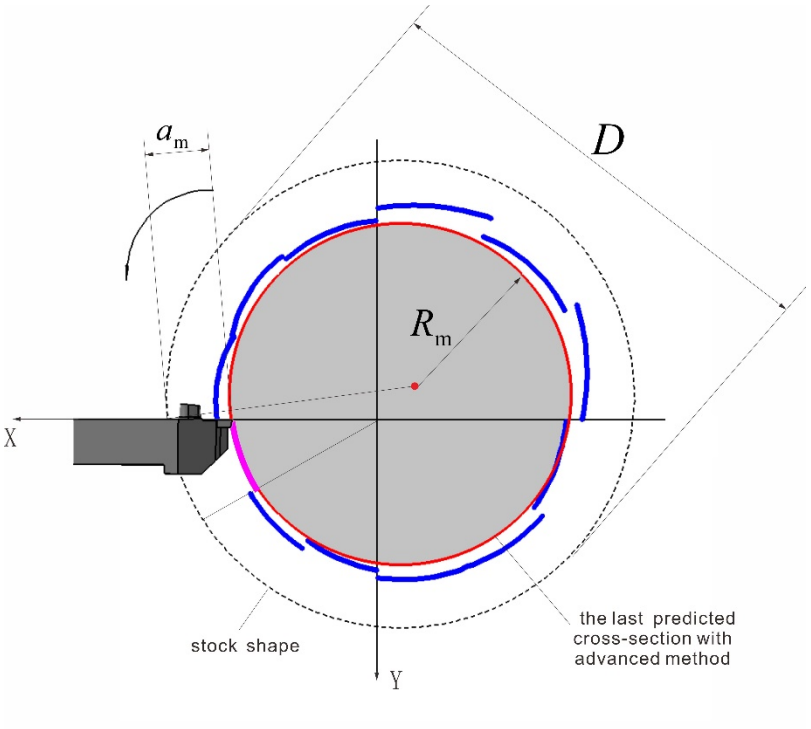

Fig 4.14 The last stage in the first feed per revolution

4.8 The prediction of the diametrical deviation along the shaft

With the method above, the diameter along the whole slender shaft can be obtained.

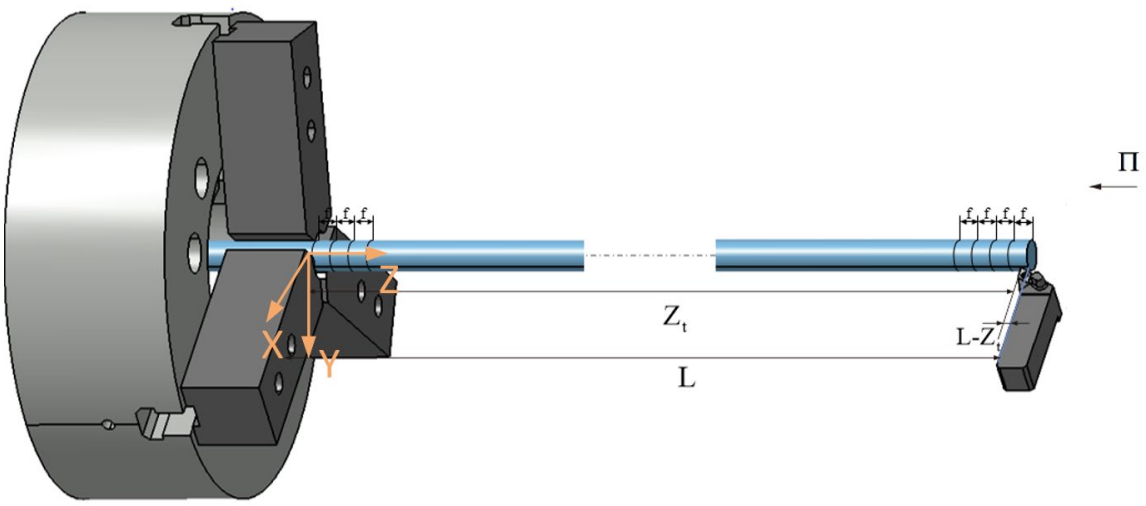

Fig 4.15 Prediction of the diameter error along the whole slender shaft

For the x stage of the y feed per revolution as shown in Fig 4.14 and a_x^y is the depth of cut. It is obtained as:

$$a_x^y = \frac{D}{2} - R_{x-1}^y$$

Eq. 4.62

If $x = 1$, then

$$a_1^y = \frac{D}{2} - R_{my-m}^{y-1}$$

Eq. 4.63

The cutting force components in the third stage is shown below:

$$F_{tx}^y = F_t(a_x^y)$$

Eq. 4.64

$$F_{rx}^y = F_r(a_x^y)$$

Eq. 4.65

The radial deviation in the third stage can be written as:

$$\delta_x^y = g(F_{tx}^y, F_{rx}^y, Z_{tx}^y, Z_s)$$

Eq. 4.66

where,

$$Z_{tx}^{y} = (y - 1 + \frac{x\alpha}{360}) \cdot f$$

Eq. 4.67

The change in element number must be noted as the tool travels and locates at the left of the steady rest. Then, the radius of the cross-section at the end of the second stage can be written as:

$$R_{x}^{y} = \frac{D}{2} - \delta_{x}^{y}$$

Eq. 4.68

In addition to the above derivation, the model can also be modified to accommodate lathes with tool-following type steady rest. These types of lathes are usually older machines. As the tool moves along the shaft axis, the steady rest will follow it and the distance between the tool and the steady rest is a constant L_s. The stead rest is usually on the right of the tool. Thus, in this case, the Z coordinates of the steady rest can be calculated as

$$Z_s = Z_t + L_s$$

Eq. 4.69

Chapter 5 Verification and discussion

5.1 Verification of the novel model

To demonstrate the feasibility of this novel approach over the existing model, this approach is applied to an experimental model. In the published paper [8], an experiment for predicting the

diameter error in slender shaft turning has been done. The experiment set-up is shown in Fig 3.3. The geometric feature of the slender shaft is shown below:

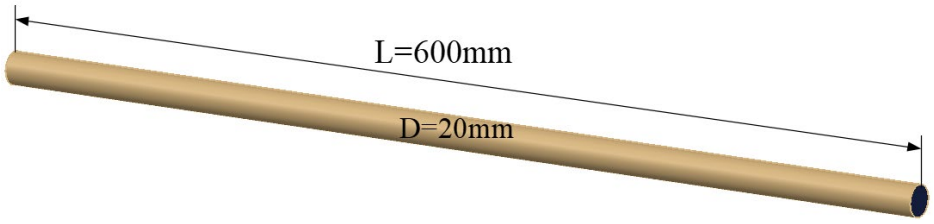

Fig 5.1 The slender shaft geometric feature

The material parameters and cutting parameters are shown below:

Table 5.1 Material parameters and cutting parameters

Material	Young's modulus	Poisson's ratio	Density	Cutting depth	Feed rate	Cutting speed
1045steel	205GPa	0.3	7.85g/cm³	1.5mm	0.5mm/r	0.524m/s

The stiffness of the steady rest are:

Table 5.2 Stiffness of the steady rest

X	Y
8.93×10^3N/mm	4.06×10^4N/mm

And the distance between the cutting tool and the steady rest remains 10mm.

By using the new approach, the diametrical deviation along this slender shaft in the same turning process has been calculated. The result is plotted in Fig 5.2 with the experimental results. It can be seen that the two sets of results show good agreement in the pattern. The maximum difference between the two sets of results are at Z = 300 mm, where it is the midpoint of the shaft. The difference is about 0.007mm and the relative error is about 11%. This error can be assumed to be the error induced during the experiment. The comparison here shows the developed model is valid.

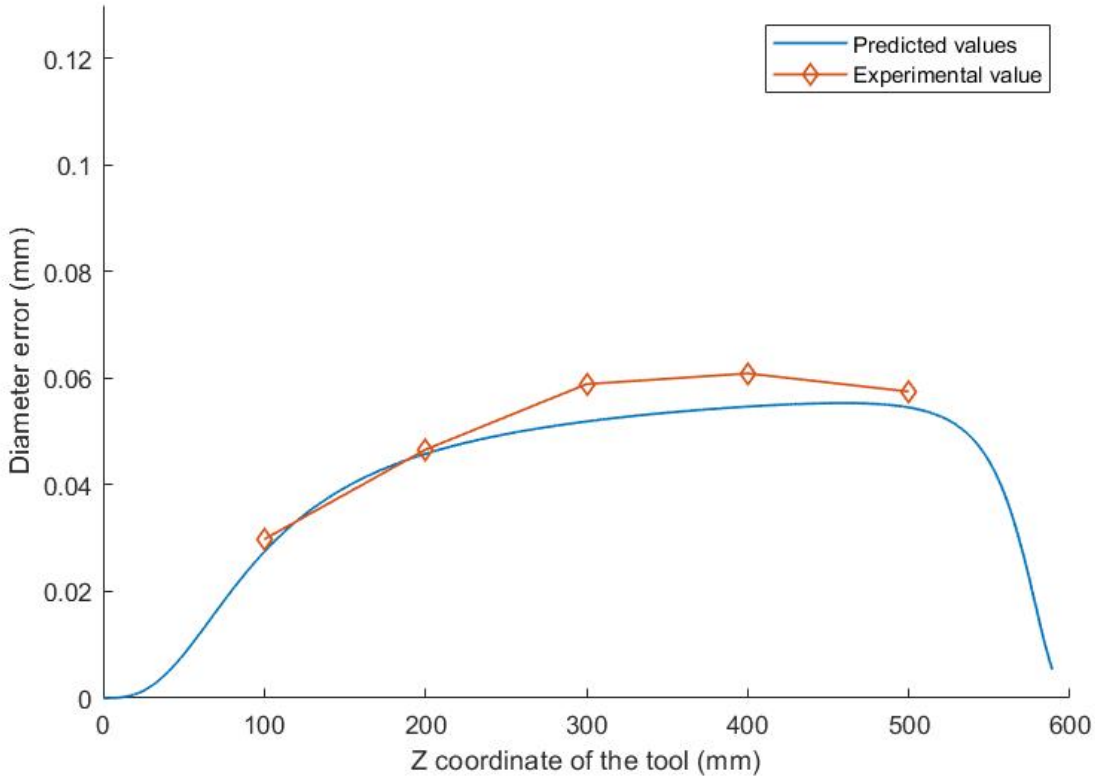

Fig 5.2 The comparison between the results obtained by the new approach and experiment

5.2 Discussion of the novel model

5.2.1 Application of the high strength material

In the case above, 1045steel is used as the material of the slender shaft. This material is neither expensive nor is difficult to machine. However, when the expensive and difficult-to-cut materials are concerned, the diametrical deviation in slender shaft turning should be predicted very precisely. In order to see the improvement that the novel approach would make, a high strength material is taken as an example. The predicted results are calculated with the traditional and novel methods. The geometric feature of the slender shaft in this case is shown in Fig 5.1.

The material parameters and the cutting parameters are shown below:

Table 5.3 Material parameters and cutting parameters

Material	Young's modulus	Poisson's ratio	Density	Cutting depth	Feed rate	Cutting speed
40CrNi2Si2MoVA	600GPa	0.3	8.36g/cm³	3mm	1mm/r	1m/s

The stiffness of the steady rest are:

Table 5.4 Stiffness of the steady rest

X	Y
8.93×10^3N/mm	4.06×10^4N/mm

To compare with the traditional methods, the tool-following steady rest is employed in our model. And the distance between the cutting tool and the steady rest remains 10mm. The calculated results are plot in Fig 5.3.

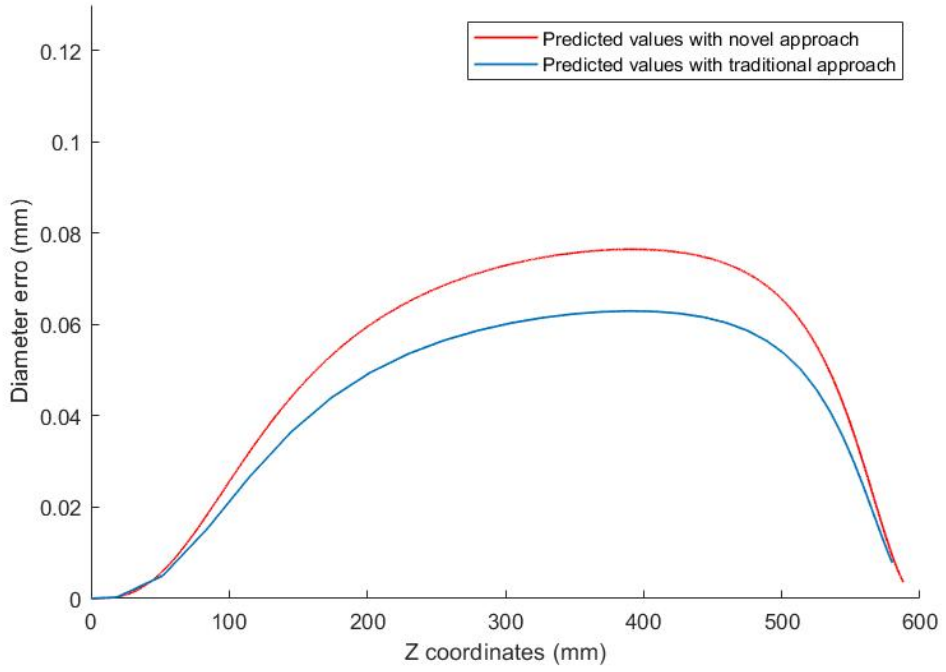

Fig 5.3 The comparison between the results obtained with the novel approach and the traditional approach

From Fig 5.3, it can be seen that the difference between the results obtained with the novel approach and the traditional approach is about 0.018mm. Since the part with this material is usually designed with a tight tolerance requirement. An error of 0.018mm could disqualify the part and thus it cannot be ignored.

The difference between these two methods originates from the following fact. The novel method has taken the change of the depth of cut and cutting force into account. Meanwhile, the traditional methods consider the cutting force a constant. From the machining point-of-view, when machining the difficult-to-cut material, the cutting forces are sensitive to the change of the depth of cut. This is the reason why from Fig 5.3, the novel method predicts larger diametrical deviations.

5.2.2 Application when the position of the steady rest is fixed

In the above examples and discussion, modifications to the novel model have been made so that the steady rest remains 10mm to the tool. The reason for that is to make a comparison with the traditional methods. In most situations in modern manufacturing, the steady rest is installed on the rail of the lathe and can be positioned at any position along the shaft. However, once the position of the steady rest is determined and the hydraulic pressure is applied. The steady rest does not change its position. Thus, during the turning process, the distance between the tool and the steady rest will change. In this section, a numerical example is given to predict the diametrical deviation of a slender shaft in this practical scenario.

In this example, the steady rest is fixed at 300mm along the Z-axis. The material parameters and the cutting parameters are listed in Table 5.1 and the stiffness of the steady rest is listed in Table 5.2. The results obtained with the novel approach is plotted in Fig 5.4.

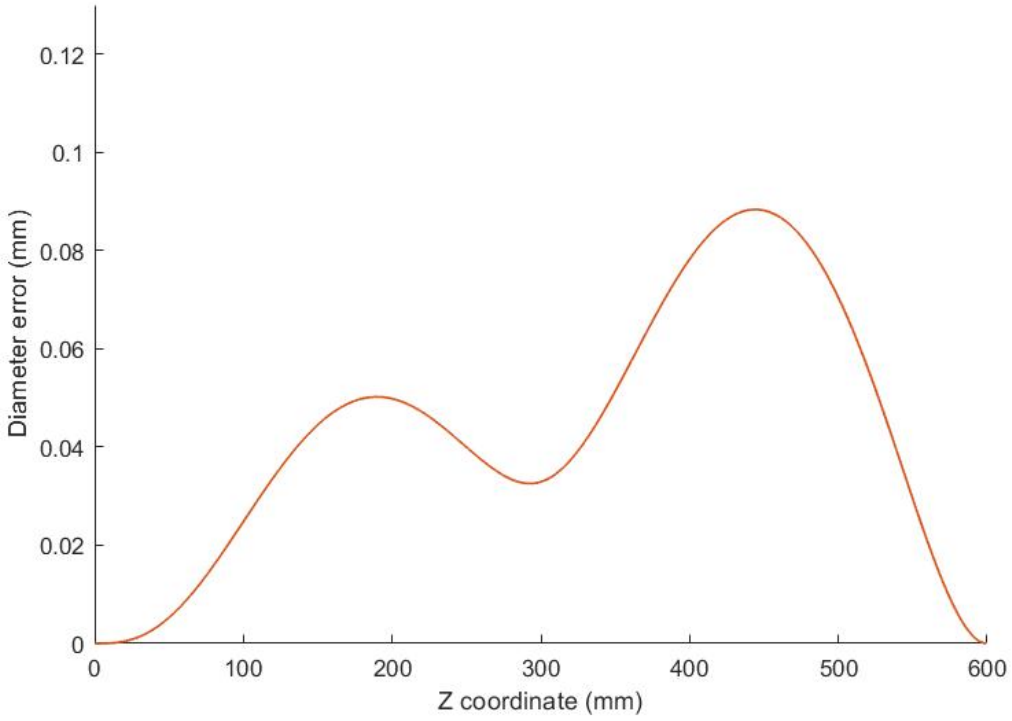

Fig 5.4 The diametrical deviation predicted with novel approach when the steady rest is fixed at 300mm along Z-axis

It is shown that there is an obvious trough at the steady rest position when the steady rest is fixed. This is very different from the situation when the steady rest moves with the tool. And this provides a result much closer to the real machining situation. Oblivion to these characteristics can lead to potential part damage. Thus, it is necessary to build a model for predicting the diametrical deviation for slender shafts turning with the steady rest fixed.

5.3 An application for Featured Slender Shafts Turning Process

5.3.1 Establish of the generic model for featured slender shafts

In practice, the slender shafts can also have many different features, such as being hollow, multi-diameters, and having fillets, threads, and holes. To machine such shafts, their features must be considered, since these features affect the overall shaft rigidity. Unfortunately, previous research mainly focused on turning, a solid, smooth, and uniform slender shaft. Therefore, it is necessary to develop a computational method for the featured slender shaft.

Multi-diameter shafts have largely different rigidity in the parts with different parameters. Especially, when the shafts are hollow, the rigidity difference is even more noticeable at different diameters. Therefore, as a generic model to predict diametrical deviation for the featured slender shafts, a multi-diameter, hollow shaft is studied.

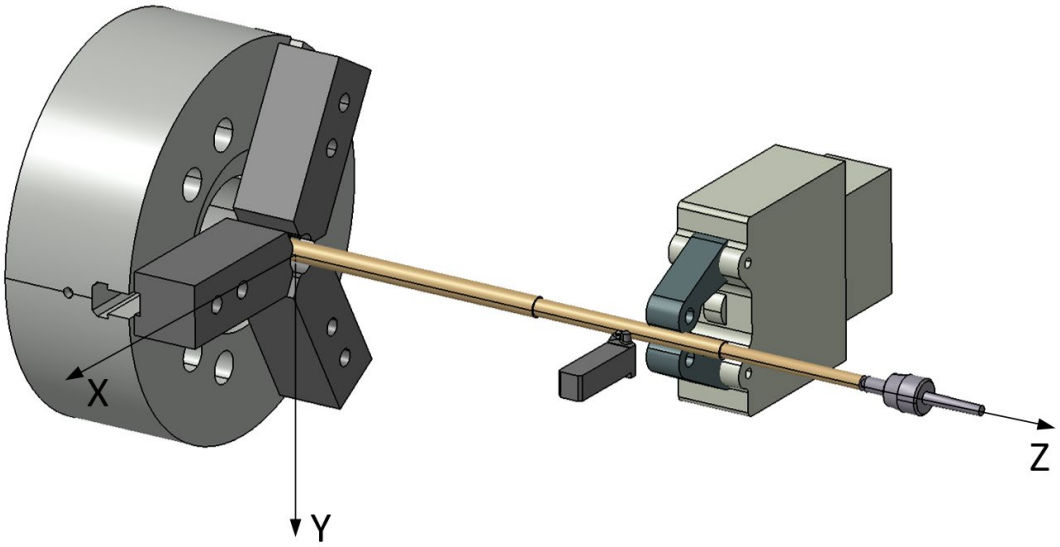

Fig 5.5 Turning process of a multi-diameter hollow slender shaft

Compared to the “perfect” slender shaft with the uniform cross-section along Z-axis, the featured slender shafts need to be considered more changes of the cross-section geometric features axially, along Z-direction. These differences will reflect in the stiffness matrix since the stiffness

matrix is directly related to the slender shaft properties in the stiffness function. The members of the stiffness matrix include Young's modulus E, the moment of inertia I, and lengths of each element L. Mostly, a slender shaft is made in one material, so Young's modulus E remains the same during machining. And the slender shaft geometric features change does not influence the Young's modulus E. However, the moment of inertia I at different positions along the shaft depends on the shape of the cross-section. This will be modified by the slender shaft geometric features change. L depends on how the slender shaft is discretized.

In summary, in order to consider the cross-section geometric features, the change in the moment of inertia I must be considered. And it will cause the change of the quantity and the value of element stiffness matrixes. Thus the overall stiffness matrix K representing the physical features of the slender shaft needs to be modified as well.

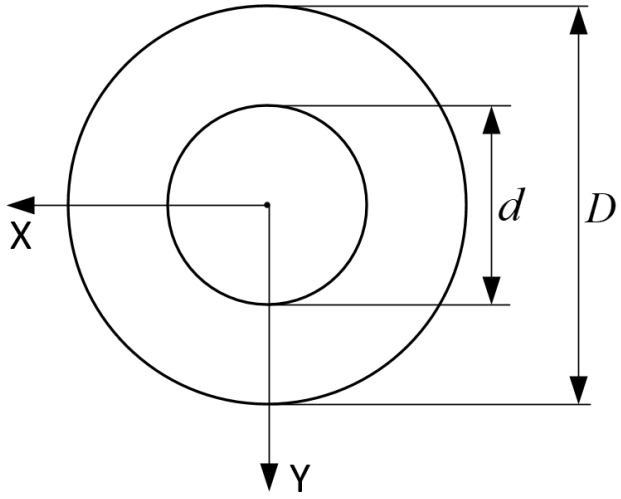

Fig 5.6 A cross-section of the multi-diameter hollow slender shaft

Fig 4.2 shows a cross-section picked randomly from the multi-diameter slender shaft. The diameter of the hollow part is d. The diameter of the slender shaft is D. According to the mechanics of materials [25], the moment of inertia of this cross-section is:

$$I=\frac{\pi D^4}{64}(1-\alpha^4)$$

Eq. 5.1

where,

$$\alpha=\frac{d}{D}$$

Eq. 5.2

The FEA method described in Chapter 3 is extended in this chapter. To facilitate the FEA method, a new discretization scheme must be established. Since the cross-section changes axially, a node should be set at the position where the cross-sectional diameter changes. In addition, four nodes are set at the chuck, the steady rest, the tool, and the tailstock respectively (see Fig 5.7). In Fig 5.7, Z_t is the position of the tool and Z_r is the position of the steady rest. The multi-diameter shaft has diameters from D_1 to D_s and its length is L. As a result of such discretization, both the quantities of the elements and nodes will be different from that of Chapter 3. The stiffness matrix for each element should respect its own moment of inertia. Therefore, the overall stiffness matrix becomes complicated.

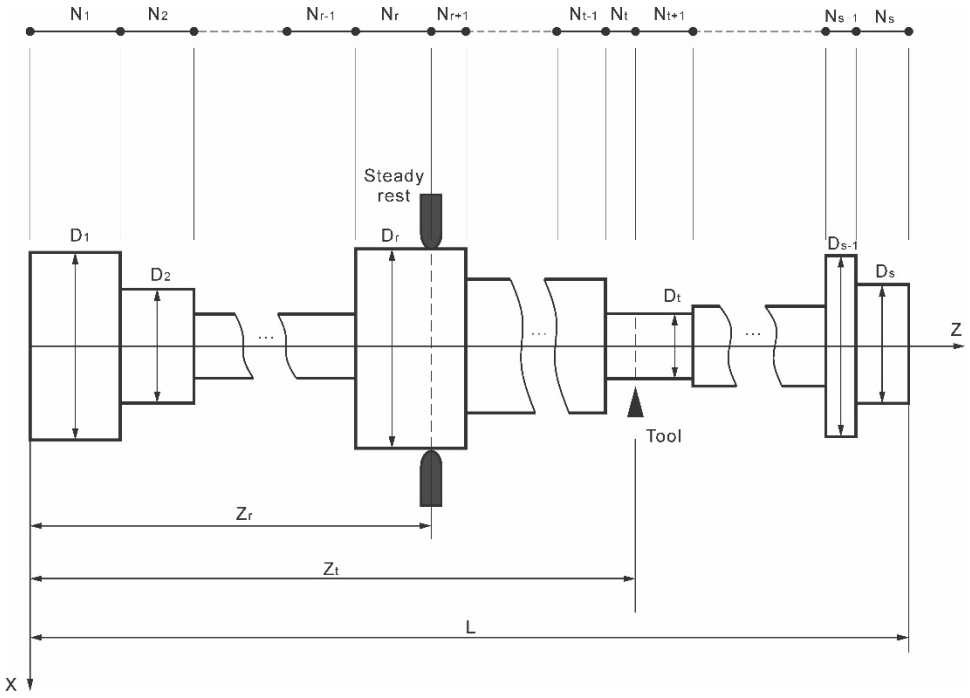

Fig 5.7 Discretization of a generic multi-diameter hollow shaft

To illustrate the generic model, an example is used to explain the derivation process.

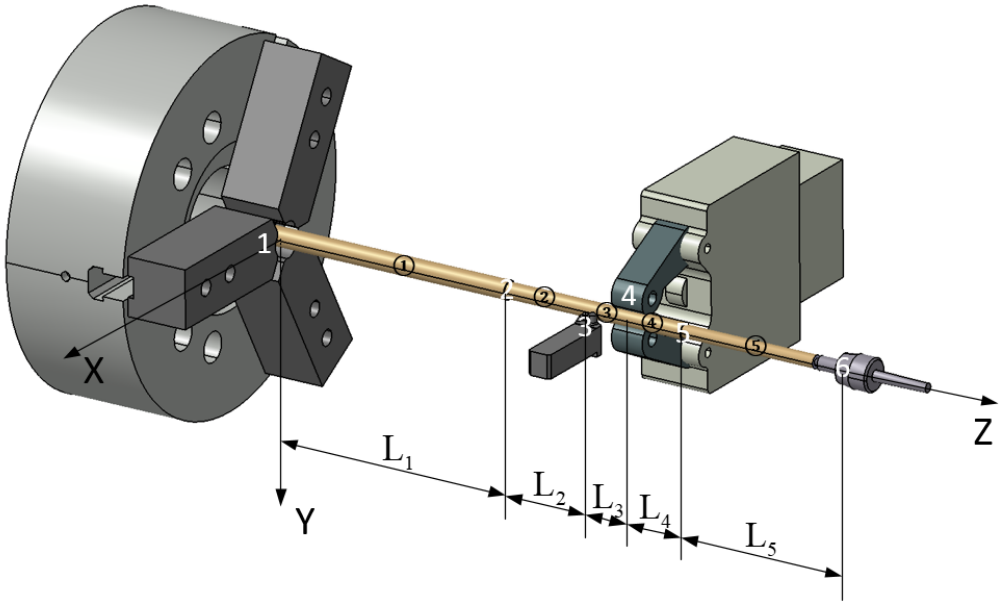

Fig 5.8 Discretization of a multi-diameter hollow slender shaft

In Fig 5.8, the workpiece is a multi-diameter hollow slender shaft with three different diameters. And the diameter of the hollow part remains the same. Therefore, there are three different moments of inertia appear in this slender shaft calculated with Eq. 5.1 and Eq. 5.2, namely I_1, I_2, I_3, and three different cross-sections correspond to three different lengths. Consider the chuck, the tool, the steady rest, and the tailstock, the discretization is illustrated in Fig 5.8. The overall stiffness matrix function in the X and Y directions is:

$$\begin{bmatrix} u_{1x} \\ \theta_{1x} \\ u_{2x} \\ \theta_{2x} \\ u_{3x} \\ \theta_{3x} \\ u_{4x} \\ \theta_{4x} \\ u_{5x} \\ \theta_{5x} \\ u_{6x} \\ \theta_{6x} \end{bmatrix} = \begin{bmatrix} \frac{12EI_1}{L_1^3} & \frac{6EI_1}{L_1^2} & -\frac{12EI_1}{L_1^3} & \frac{6EI_1}{L_1^2} & 0 & 0 & 0 & 0 & 0 & 0 & 0 & 0 \\ \frac{6EI_1}{L_1^2} & \frac{4EI_1}{L_1} & -\frac{6EI_1}{L_1^2} & \frac{2EI_1}{L_1} & 0 & 0 & 0 & 0 & 0 & 0 & 0 & 0 \\ -\frac{12EI_1}{L_1^3} & -\frac{6EI_1}{L_1^2} & \frac{12EI_1}{L_1^3}+\frac{12EI_2}{L_2^3} & -\frac{6EI_1}{L_1^2}+\frac{6EI_2}{L_2^2} & -\frac{12EI_2}{L_2^3} & \frac{6EI_2}{L_2^2} & 0 & 0 & 0 & 0 & 0 & 0 \\ \frac{6EI_1}{L_1^2} & \frac{2EI_1}{L_1} & -\frac{6EI_1}{L_1^2}+\frac{6EI_2}{L_2^2} & \frac{4EI_1}{L_1}+\frac{4EI_2}{L_2} & -\frac{6EI_2}{L_2^2} & \frac{6EI_2}{L_2^2} & 0 & 0 & 0 & 0 & 0 & 0 \\ 0 & 0 & -\frac{12EI_2}{L_2^3} & -\frac{6EI_2}{L_2^2} & \frac{12EI_2}{L_2^3}+\frac{12EI_3}{L_3^3} & -\frac{6EI_2}{L_2^2}+\frac{6EI_3}{L_3^2} & -\frac{12EI_3}{L_3^3} & \frac{6EI_3}{L_3^2} & 0 & 0 & 0 & 0 \\ 0 & 0 & \frac{6EI_2}{L_2^2} & \frac{2EI_2}{L_2} & -\frac{6EI_2}{L_2^2}+\frac{6EI_3}{L_3^2} & \frac{4EI_2}{L_2}+\frac{4EI_3}{L_3} & -\frac{6EI_3}{L_3^2} & \frac{2EI_3}{L_3} & 0 & 0 & 0 & 0 \\ 0 & 0 & 0 & 0 & -\frac{12EI_3}{L_3^3} & -\frac{6EI_3}{L_3^2} & \frac{12EI_3}{L_3^3}+\frac{12EI_4}{L_4^3} & -\frac{6EI_3}{L_3^2}+\frac{6EI_4}{L_4^2} & -\frac{12EI_4}{L_4^3} & \frac{6EI_4}{L_4^2} & 0 & 0 \\ 0 & 0 & 0 & 0 & \frac{6EI_3}{L_3^2} & \frac{2EI_3}{L_3} & \frac{12EI_3}{L_3^3}+\frac{12EI_4}{L_4^3} & \frac{4EI_3}{L_3}+\frac{4EI_4}{L_4} & -\frac{6EI_4}{L_4^2} & \frac{2EI_4}{L_4} & 0 & 0 \\ 0 & 0 & 0 & 0 & 0 & 0 & -\frac{12EI_4}{L_4^3} & -\frac{6EI_4}{L_4^2} & \frac{12EI_4}{L_4^3}+\frac{12EI_5}{L_5^3} & -\frac{6EI_4}{L_4^2}+\frac{6EI_5}{L_5^2} & -\frac{12EI_5}{L_5^3} & \frac{6EI_5}{L_5^2} \\ 0 & 0 & 0 & 0 & 0 & 0 & \frac{6EI_4}{L_4^2} & \frac{2EI_4}{L_4} & \frac{12EI_4}{L_4^3}+\frac{12EI_5}{L_5^3} & \frac{4EI_4}{L_4}+\frac{4EI_5}{L_5} & -\frac{6EI_5}{L_5^2} & \frac{2EI_5}{L_5} \\ 0 & 0 & 0 & 0 & 0 & 0 & 0 & 0 & -\frac{12EI_5}{L_5^3} & -\frac{6EI_5}{L_5^2} & \frac{12EI_5}{L_5^3} & -\frac{6EI_5}{L_5^2} \\ 0 & 0 & 0 & 0 & 0 & 0 & 0 & 0 & \frac{6EI_5}{L_5^2} & \frac{2EI_5}{L_5} & -\frac{6EI_5}{L_5^2} & \frac{4EI_5}{L_5} \end{bmatrix}^{-1} \begin{bmatrix} F_{1x} \\ M_{1x} \\ F_{2x} \\ M_{2x} \\ F_{3x} \\ M_{3x} \\ F_{4x} \\ M_{4x} \\ F_{5x} \\ M_{5x} \\ F_{6x} \\ M_{6x} \end{bmatrix}$$

Eq. 5.3

$$\begin{bmatrix} u_{1y} \\ \theta_{1y} \\ u_{2y} \\ \theta_{2y} \\ u_{3y} \\ \theta_{3y} \\ u_{4y} \\ \theta_{4y} \\ u_{5y} \\ \theta_{5y} \\ u_{6y} \\ \theta_{6y} \end{bmatrix} = \begin{bmatrix} \frac{12EI_1}{L_1^3} & \frac{6EI_1}{L_1^2} & -\frac{12EI_1}{L_1^3} & \frac{6EI_1}{L_1^2} & 0 & 0 & 0 & 0 & 0 & 0 & 0 & 0 \\ \frac{6EI_1}{L_1^2} & \frac{4EI_1}{L_1} & -\frac{6EI_1}{L_1^2} & \frac{2EI_1}{L_1} & 0 & 0 & 0 & 0 & 0 & 0 & 0 & 0 \\ -\frac{12EI_1}{L_1^3} & -\frac{6EI_1}{L_1^2} & \frac{12EI_1}{L_1^3}+\frac{12EI_2}{L_2^3} & -\frac{6EI_1}{L_1^2}+\frac{6EI_2}{L_2^2} & -\frac{12EI_2}{L_2^3} & \frac{6EI_2}{L_2^2} & 0 & 0 & 0 & 0 & 0 & 0 \\ \frac{6EI_1}{L_1^2} & \frac{2EI_1}{L_1} & -\frac{6EI_1}{L_1^2}+\frac{6EI_2}{L_2^2} & \frac{4EI_1}{L_1}+\frac{4EI_2}{L_2} & -\frac{6EI_2}{L_2^2} & \frac{6EI_2}{L_2^2} & 0 & 0 & 0 & 0 & 0 & 0 \\ 0 & 0 & -\frac{12EI_2}{L_2^3} & -\frac{6EI_2}{L_2^2} & \frac{12EI_2}{L_2^3}+\frac{12EI_3}{L_3^3} & -\frac{6EI_2}{L_2^2}+\frac{6EI_3}{L_3^2} & -\frac{12EI_3}{L_3^3} & \frac{6EI_3}{L_3^2} & 0 & 0 & 0 & 0 \\ 0 & 0 & \frac{6EI_2}{L_2^2} & \frac{2EI_2}{L_2} & -\frac{6EI_2}{L_2^2}+\frac{6EI_3}{L_3^2} & \frac{4EI_2}{L_2}+\frac{4EI_3}{L_3} & -\frac{6EI_3}{L_3^2} & \frac{2EI_3}{L_3} & 0 & 0 & 0 & 0 \\ 0 & 0 & 0 & 0 & -\frac{12EI_3}{L_3^3} & -\frac{6EI_3}{L_3^2} & \frac{12EI_3}{L_3^3}+\frac{12EI_4}{L_4^3} & -\frac{6EI_3}{L_3^2}+\frac{6EI_4}{L_4^2} & -\frac{12EI_4}{L_4^3} & \frac{6EI_4}{L_4^2} & 0 & 0 \\ 0 & 0 & 0 & 0 & \frac{6EI_3}{L_3^2} & \frac{2EI_3}{L_3} & \frac{12EI_3}{L_3^3}+\frac{12EI_4}{L_4^3} & \frac{4EI_3}{L_3}+\frac{4EI_4}{L_4} & -\frac{6EI_4}{L_4^2} & \frac{2EI_4}{L_4} & 0 & 0 \\ 0 & 0 & 0 & 0 & 0 & 0 & -\frac{12EI_4}{L_4^3} & -\frac{6EI_4}{L_4^2} & \frac{12EI_4}{L_4^3}+\frac{12EI_5}{L_5^3} & -\frac{6EI_4}{L_4^2}+\frac{6EI_5}{L_5^2} & -\frac{12EI_5}{L_5^3} & \frac{6EI_5}{L_5^2} \\ 0 & 0 & 0 & 0 & 0 & 0 & \frac{6EI_4}{L_4^2} & \frac{2EI_4}{L_4} & \frac{12EI_4}{L_4^3}+\frac{12EI_5}{L_5^3} & \frac{4EI_4}{L_4}+\frac{4EI_5}{L_5} & -\frac{6EI_5}{L_5^2} & \frac{2EI_5}{L_5} \\ 0 & 0 & 0 & 0 & 0 & 0 & 0 & 0 & -\frac{12EI_5}{L_5^3} & -\frac{6EI_5}{L_5^2} & \frac{12EI_5}{L_5^3} & -\frac{6EI_5}{L_5^2} \\ 0 & 0 & 0 & 0 & 0 & 0 & 0 & 0 & \frac{6EI_5}{L_5^2} & \frac{2EI_5}{L_5} & -\frac{6EI_5}{L_5^2} & \frac{4EI_5}{L_5} \end{bmatrix}^{-1} \begin{bmatrix} F_{1y} \\ M_{1y} \\ F_{2y} \\ M_{2y} \\ F_{3y} \\ M_{3y} \\ F_{4y} \\ M_{4y} \\ F_{5y} \\ M_{5y} \\ F_{6y} \\ M_{6y} \end{bmatrix}$$

Eq. 5.4

To expand these functions to a more generic slender shaft, with more cross-sections, one only needs to change the quantity of discretized elements and the scale of the overall stiffness matrix.

5.3.2 An example of the generic model for a featured slender shaft

A multi-diameter hollow slender shaft is shown in Fig 5.9 and the geometric feature is given.

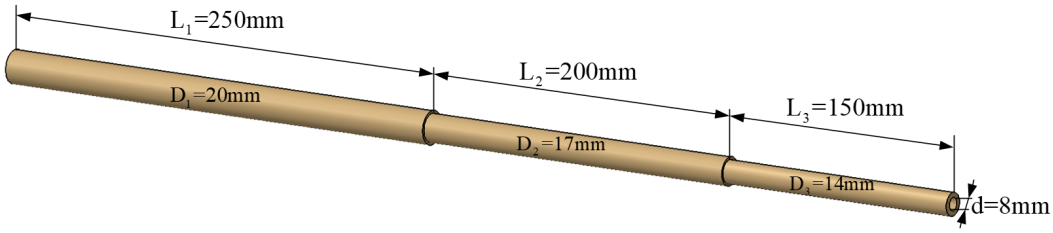

Fig 5.9 A multi-diameter hollow slender shaft

The material parameters and the cutting parameters are listed in Table 5.1 and the stiffness of the steady rest are listed in Table 5.2. The steady rest step up at 300mm along the Z-axis. The result is plotted below:

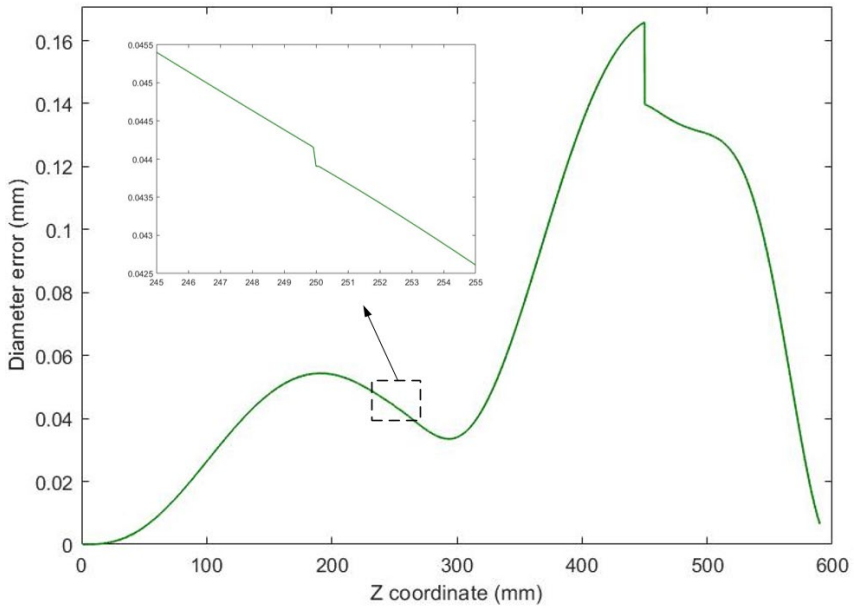

Fig 5.10 The result for predicting the diameter error in the turning process of the multi-diameter hollow slender shaft

It can be observed from the figure that two sudden changes occur at 250mm and 450mm along Z-axis. These positions correspond to the two steps on the slender shaft. The spikes at 450 mm are about 0.04 mm and the spikes at 250mm are about 0.001mm. The spikes at 450mm are more noticeable due to two main reasons: 1) the cross-sectional at $Z_t = 450mm$ is between 14 and 17mm, compared to 17 to 20 mm at $Z_t = 250mm$. So the part is less rigid at 450mm. 2) the spikes at 250mm is close to the position of the steady rest, which locates at $Z_r = 300mm$. So the rigidity of the part is higher at 250mm. Additionally, from Fig 5.10, a trough at 300 mm can be noticed. This is the steady rest position. Since the steady rest provides additional supports, the diametrical deviation of the shaft decreases at 300mm. Overall, the diametrical deviation ranges from 0 to 0.16mm. This is because the slender shaft is hollow and the part is more prone to deflect.

Chapter 6 Conclusion and Future Work

6.1 Conclusion

In summary, a novel numerical model for predicting the diametrical error in slender shaft turning considered the change of depth of cut and the cutting force in different moments during the turning process and other possible varieties has been proposed here.

Three conclusions are summed up based on three studied cases:

1. When the slender shaft is made of a high-strength and difficult-to-machine material, it is important to consider and compensate the diametrical errors due to the dynamic and continuous coupling between the depth of cut and the cutting force, because when machining this kind of materials, the cutting force is sensitive to the depth of cut.
2. As in the modern turning process, the steady rest is not able to move with the cutting tool, the change of the distance between the cutting tool and the steady rest needs to be considered in the algorithm. In this situation, the diametrical error would exist an obvious trough at the position of the steady rest.
3. For shafts with features, like the multi-diameter hollow slender shaft, it is necessary to consider these features when calculate and compensate the diametrical error in the turning process, as the geometric features of the slender shaft greatly influence diametrical errors in different positions. Specifically, when machining a hollow slender shaft, the general diametrical error in the turning process is higher compared with the solid slender shaft because hollow leads to low rigidity. And at the position where the diameter of the cross-sections changes suddenly, the diametrical error would change suddenly as well.

6.2 Recommendations for future work

Although the results and conclusions are very logical and reasonable from the view of theories in mechanics and machining, experiments of the cases studied in this work still need to be done to verify the accuracy of the novel approach for predicting the diametrical error in the turning process.

Besides, in order to apply this approach in real manufacturing, it is necessary to combine the algorithm and CNC program to compensate the diametrical errors of slender shafts in the turning process.

Bibliography

[1] Phan, A.V., Cloutier, G. and Mayer, J.R.R., 1999. A finite-element model with closed-form solutions to workpiece deflections in turning. International Journal of Production Research, 37(17), pp.4039-4051.

[2] Smid, Peter. CNC programming handbook: a comprehensive guide to practical CNC programming. Industrial Press Inc., 2003.

[3] Moaveni, Saeed. Finite element analysis theory and application with ANSYS, 3/e. Pearson Education India, 2011.

[4] Smid, Peter. CNC control setup for milling and turning: mastering CNC control systems. Industrial Press Inc., 2010.

[5] Black, J. Temple, and Ronald A. Kohser. DeGarmo's materials and processes in manufacturing. John Wiley & Sons, 2020.

[6] Mayer, J.R., Phan, A.V. and Cloutier, G., 2000. Prediction of diameter errors in bar turning: a computationally effective model. Applied Mathematical Modelling, 24(12), pp.943-956.

[7] Stephenson, D.A. and Bandyopadhyay, P., 1997. Process-independent force characterization for metal-cutting simulation.

[8] Cui, B. and Han, R., 2008, June. Modeling of dimensional errors in slender bar turning using artificial neural networks. In 2008 7th World Congress on Intelligent Control and Automation (pp. 6053-6056). IEEE.

[9] Kops, L., Gould, M. and Mizrach, M., 1993. Improved analysis of the workpiece accuracy in turning, based on the emerging diameter.

[10] Yang, S., Yuan, J. and Ni, J., 1997. Real-time cutting force induced error compensation on a turning center. International Journal of Machine Tools and Manufacture, 37(11), pp.1597-1610.

[11] Jianliang, G. and Rongdi, H., 2006. A united model of diametral error in slender bar turning with a follower rest. International Journal of Machine Tools and Manufacture, 46(9), pp.1002-1012.

[12] Carrino, L., Giorleo, G., Polini, W. and Prisco, U., 2002. Dimensional errors in longitudinal turning based on the unified generalized mechanics of cutting approach.: Part II: Machining process analysis and dimensional error estimate. International Journal of Machine Tools and Manufacture, 42(14), pp.1517-1525.

[13] Wilhelm, R.G., Srinivasan, N., Farabaugh, F. and Hocken, R., 1997. Part form errors predicted from machine tool performance measurements. CIRP Annals, 46(1), pp.471-474.

[14] Polini, W. and Prisco, U., 2003. The estimation of the diameter error in bar turning: a comparison among three cutting force models. The International Journal of Advanced Manufacturing Technology, 22(7-8), pp.465-474.

[15] Shawky, A.M. and Elbestawi, M.A., 1998. Model-based predictive control of workpiece accuracy in bar turning.

[16] Fan, C., Collins Jr, E.G., Liu, C. and Wang, B., 2003. Radial error feedback control for bar turning in CNC turning centers. J. Manuf. Sci. Eng., 125(1), pp.77-84.

[17] Cui, B.D. and Guo, J.L., 2009. Modeling of dimensional errors in slender bar turning process using artificial neural networks. In Applied Mechanics and Materials (Vol. 16, pp. 549-553). Trans Tech Publications Ltd.

[18] Phan, A.V., Baron, L., Mayer, J.R.R. and Cloutier, G., 2003. Finite element and experimental studies of diametral errors in cantilever bar turning. Applied Mathematical Modelling, 27(3), pp.221-232.

[19] Kops, L., Gould, M. and Mizrach, M., 1994. A search for equilibrium between workpiece deflection and depth of cut: key to predictive compensation for deflection in turning. ASME-PUBLICATIONS-PED, 68, pp.819-819.

[20] J.T Black, Ronald A.Kohser. Material and process in manufacturing (2008):598.

[21] Stephenson, D.A. and Bandyopadhyay, P., 1997. Process-independent force characterization for metal-cutting simulation.

[22] Gu, F., Kapoor, S.G., DeVor, R.E. and Bandyopadhyay, P., 1991. An approach to on-line cutter runout estimation in face milling. Transactions of NAMRI/SME, 19, pp.240-247.

[23] Kline, W.A., 1982. THE PREDICTION OF CUTTING FORCES AND SURFACE ACCURACY FOR THE END MILLING PROCESS.

[24] Stewart, James, Daniel K. Clegg, and Saleem Watson. Calculus: early transcendentals. Cengage Learning, 2020.

[25] R.C., Hibbeler, 2001. MECHANICS OF MATERIALS.

[26] Altintas, Y., 2000, Manufacturing Automation: Metal Cutting Mechanics, Machine Tool Vibrations, and CNC Design, Cambridge University Press, New York.